

JAMES Journal of Advances in Modeling Earth Systems*



RESEARCH ARTICLE

10.1029/2023MS004045

Key Points:

- A coupled water column biogeochemical-seabed diagenetic model is updated to include dissolved inorganic carbon (DIC) and TAlk for ocean acidification
- The modeled impact of benthic fluxes on bottom water acidification during quiescent periods is impacted by the intensity of bio-diffusion
- Resuspension enhances bottom water acidification by increasing the benthic flux DIC/TAlk ratio

Supporting Information:

Supporting Information may be found in the online version of this article.

Correspondence to:

D. Yin and C. K. Harris, dyin@vims.edu; ckharris@vims.edu

Citation:

Yin, D., Cui, L., Harris, C. K., Moriarty, J. M., Beck, H., & Maiti, K. (2024). The role of benthic fluxes in acidifying the bottom waters in the Northern Gulf of Mexico hypoxic zone based on an updated water column biogeochemical-seabed diagenetic and sediment transport model. *Journal of Advances in Modeling Earth Systems*, 16, e2023MS004045. https://doi.org/10.1029/2023MS004045

Received 28 SEP 2023 Accepted 21 AUG 2024

Author Contributions:

Conceptualization: Dongxiao Yin, Courtney K. Harris Data curation: Dongxiao Yin Formal analysis: Dongxiao Yin Funding acquisition: Courtney K. Harris, Kanchan Maiti

© 2024 The Author(s). Journal of Advances in Modeling Earth Systems published by Wiley Periodicals LLC on behalf of American Geophysical Union. This is an open access article under the terms of the Creative Commons Attribution-NonCommercial-NoDerivs License, which permits use and distribution in any medium, provided the original work is properly cited, the use is non-commercial and no modifications or adaptations are made.

The Role of Benthic Fluxes in Acidifying the Bottom Waters in the Northern Gulf of Mexico Hypoxic Zone Based on an Updated Water Column Biogeochemical-Seabed Diagenetic and Sediment Transport Model

Dongxiao Yin¹, Linlin Cui¹, Courtney K. Harris¹, Julia M. Moriarty², Hannah Beck³, and Kanchan Maiti³

¹Virginia Institute of Marine Science, William & Mary, Gloucester Point, VA, USA, ²Department of Atmospheric and Oceanic Sciences and Institute of Arctic and Alpine Research, University of Colorado Boulder, Boulder, CO, USA,

Abstract The seabed and the water column are tightly coupled in shallow coastal environments. Numerical models of seabed-water interaction provide an alternative to observational studies that require concurrent measurements in both compartments, which are hard to obtain and rarely available. Here, we present a coupled model that includes water column biogeochemistry, seabed diagenesis, sediment transport and hydrodynamics. Our model includes realistic representations of biogeochemical reactions in both seabed and water column, and fluxes at their interface. The model was built on algorithms for seabed-water exchange in the Regional Ocean Modeling System and expanded to include carbonate chemistry in seabed. The updated model was tested for two sites where benthic flux and porewater concentration measurements were available in the northern Gulf of Mexico hypoxic zone. The calibrated model reproduced the porewater concentration-depth profiles and benthic fluxes of O2, dissolved inorganic carbon (DIC), TAlk, NO3 and NH4. We used the calibrated model to explore the role of benthic fluxes in acidifying bottom water during fair weather and resuspension periods. Under fair weather conditions, model results indicated that bio-diffusion in sediment, labile material input and sediment porosity have a large control on the importance of benthic flux to bottom water acidification. During resuspension, the model indicated that bottom water acidification would be enhanced due to the sharp increase of the DIC/TAlk ratio of benthic fluxes. To conclude, our model reproduced the seabed-water column exchange of biologically important solutes and can be used for quantifying the role of benthic fluxes in driving bottom water acidification over continental shelves.

Plain Language Summary In coastal environments where water is shallow, significant interactions occur between the seabed and the overlying water column. In the Northern Gulf of Mexico (NGoM) hypoxic zone, the seabed is believed to play an important role in the acidification of bottom ocean water. In this study we use a numerical model to understand how the seabed can affect bottom water acidification over the NGoM hypoxic zone. We found that during fair weather periods, mixing in the sediment bed due to biological activity, organic matter supply from the water column to the sediment, and the porosity of sediment itself can largely affect the role of the seabed in acidifying the bottom water. When the ocean condition is highly dynamic and resuspension occurs, the contribution of the seabed to bottom water acidification will likely be enhanced.

1. Introduction

1.1. Motivation: Benthic-Pelagic Coupling in Relation to Hypoxia and Ocean Acidification

Benthic-pelagic coupling in the aquatic environment refers to the interaction and mutual-dependence between the water column and the underlying sediment bed. The major environmental variable controlling the intensity of such coupling is the water depth (Suess, 1980). In shallow water systems including many estuaries and large portions of continental shelves, the seabed and its overlying water column are tightly coupled (Heip et al., 1995; Jorgensen et al., 1990; Roden & Tuttle, 1992). Intensive exchange of particulates and solutes occurs in such systems. For instance, the continental shelves, which cover only 7% of the surface area of the ocean, are estimated to receive 48% of the global flux of organic carbon to the seabed (Dunne et al., 2007). The subsequent benthic nutrient flux can meet around 80% of phytoplankton nutrient demand (Middelburg & Soetaert, 2004; Zhang et al., 2021). Over the Northern Gulf of Mexico (NGoM) hypoxic zone, the seabed is estimated to serve as the sink

YIN ET AL. 1 of 28

³Department of Oceanography and Coastal Sciences, Louisiana State University, Baton Rouge, LA, USA



Journal of Advances in Modeling Earth Systems

10.1029/2023MS004045

Methodology: Dongxiao Yin, Linlin Cui, Courtney K. Harris, Julia M. Moriarty, Hannah Beck, Kanchan Maiti Project administration: Courtney K. Harris, Kanchan Maiti Resources: Courtney K. Harris Software: Dongxiao Yin, Linlin Cui, Courtney K. Harris, Julia M. Moriarty Supervision: Courtney K. Harris Validation: Dongxiao Yin Visualization: Dongxiao Yin Writing - original draft: Dongxiao Yin Writing - review & editing: Dongxiao Yin, Linlin Cui, Courtney K. Harris, Julia M. Moriarty, Kanchan Maiti

for 39% of the nitrogen load from the Mississippi River watershed and release a total nitrogen flux that could provide on average 43%–66% of the sub-pycnocline, and 25%–60% of the total water column phytoplankton demand (Eldridge & Morse, 2008; Lehrter et al., 2012). Thus, knowledge of the material exchanges between the seabed and water column is of vital importance for understanding marine ecosystem functioning for this and similar regions.

Oxygen is arguably the most biologically important solute exchanged between the seabed and the water column. Sediment oxygen consumption (SOC) is believed to play a key part in promoting hypoxia development over shallow waters (Fennel & Testa, 2019). In the NGoM, the formation of hypoxia is sensitive to SOC (Fennel et al., 2013), which accounts for around 20%–30% of the total oxygen consumption within the hypoxic layers (Fennel & Testa, 2019). This contribution is reported to have been increasing over the past several decades (Turner et al., 2008). Additionally, bottom water oxygen concentration largely regulates the oxygen penetration depth in sediment and the SOC (Cai & Sayles, 1996; Rasmussen & Jørgensen, 1992). Specifically, SOC is believed to increase with bottom oxygen concentration (e.g., Murrell & Lehrter, 2011; Wang et al., 2020; Yu et al., 2015).

Observations from a few well-studied systems, including the NGoM, the Central California shelf/slope and Southern California Basin (Berelson et al., 1996; Cai et al., 2011; Hu & Cai, 2011; Hu et al., 2017; Laurent et al., 2017), show that benthic fluxes can be an important factor contributing to bottom water acidification on continental shelves. In these regions, the ratio of dissolved inorganic carbon (DIC) to total alkanility (DIC/TAlk) in the water column is close to 0.8, while that of the benthic fluxes is larger than 1 (Hu & Cai, 2011; see also Berelson et al., 1996, 2019; Cai et al., 2011; Hu et al., 2017). Thus, the benthic fluxes can potentially cause a net drop in bottom water pH. Meanwhile, the buffering capacity of seawater to ocean acidification is minimum when DIC/TAlk = 1 (Egleston et al., 2010). In this case, mixing of benthic flux with the bottom water on continental shelves is likely to lead to a weakened buffering capacity of seawater. This means a given increase in DIC will cause a larger decrease in pH. Over the NGoM hypoxic zone, Laurent et al. (2017), using a biogeochemical model, reported the recurring development of acidified water within a thin bottom layer. Wang et al. (2020), based on the analysis of a 10-year summer bottom water carbonate chemistry data set and the literature reported and recently measured benthic fluxes, found that the benthic fluxes have contributed to a pH reduction by -0.03 ± 0.04 in NGoM hypoxic zone. The pH reduction is significant (p < 0.05) in hypoxic waters. Rabouille et al. (2021) claimed that the benthic fluxes favor bottom water acidification in the NGoM hypoxic zone due to the dominance of aerobic remineralization in the seabed. However, there is still a lack of systematic understanding regarding how the benthic DIC and TAlk fluxes may vary under different environmental conditions during fair weather periods.

Resuspension frequently occurs in shallow water systems, enhancing the coupling of the benthic and pelagic compartments. Resuspension takes place when wave- and/or current-induced bed shear stresses exceed the suspension threshold of sediment, at which point sediment is eroded from the seabed and transported as suspended load within the water column. Over NGoM, the material deposited over the shallow areas of the continental shelf with water depth less than 20 m is subject to high bed stress and can be resuspended throughout the year (Allison et al., 2000; Corbett et al., 2004; Xu et al., 2011). During resuspension, a net entrainment of particulate organic matter from the seabed to the water column will be expected (Hopkinson, 1985). This may affect the remineralization of particulate organic matter, thus reshaping biogeochemical conditions in both seabed and water column. Previous observational and modeling studies for bottom boundary layers concluded that resuspension could enhance organic matter remineralization and total carbonate production (e.g., Aller, 1998; Arzayus & Canuel, 2005; Hartnett et al., 1998; Moriarty et al., 2018; Ståhlberg et al., 2006; Wainright & Hopkinson, 1997), while one study reported a decrease of the total carbonate production during resuspension (Tengberg et al., 2003). Yet former studies seldom separated the effect of resuspension on seabed versus water column processes, reporting instead overall bulk impacts. Further, little is known about the TAlk dynamics during resuspension, so that the influence of resuspension on bottom water acidification is unclear.

1.2. Goals of the Model, Objectives, and Outline of the Paper

In this study, we updated a previously developed water column biogeochemical-seabed diagenetic and sediment transport model, HydroBioSed (Moriarty et al., 2017, 2018, 2021) to include algorithms for DIC and TAlk, and more complex anaerobic processes. We applied the updated HydroBioSed in 1-D (vertical) at two sites in the

YIN ET AL. 2 of 28

NGoM hypoxic zone to resolve the sedimentary processes, while strongly nudging the overlying water conditions to observed and literature values. In this paper, we describe the subsequent developments of HydroBioSed to address the growing concern of ocean acidification and the recognized importance of benthic sources to carbonate dynamics. Our overarching goal is to provide an open-source, community-based modeling framework that can be used to advance understanding of the exchange of particulate organic matter and solutes between the seabed and water column on continental shelves and estuaries. This model can be used as a research and management tool to address issues that are strongly affected by benthic-pelagic coupling, such as hypoxia (Boynton et al., 2018; Kemp et al., 1992; Nunnally et al., 2014; Turner et al., 2008) and ocean acidification (Anthony et al., 2013; Laurent et al., 2017) in shallow coastal environments.

With this paper, we aim to (a) provide a holistic introduction of the HydroBioSed including recent updates; (b) highlight our newly added algorithms for the exchange of DIC and TAlk between the seabed and water column; and (c) understand the role of benthic DIC and TAlk fluxes in acidifying bottom water over the NGoM hypoxic zone. For this, the modeling processes represented in HydroBioSed are detailed in Section 2. In Section 3, we calibrate and evaluate our model results against recent observations of benthic fluxes and porewater concentrations over NGoM hypoxic zone. In Section 4, the sensitivity of the model results to different parameters and environmental conditions is evaluated. In Section 5, we address two research questions using NGoM as a site of interest: (a) Which processes and environmental factors are benthic fluxes of DIC and TAlk most sensitive to during fair weather periods? (b) How do episodic resuspension events impact benthic DIC and TAlk fluxes? In Section 6, we close the paper with a Summary and Conclusions.

2. Model Processes

2.1. Overview of the Development of HydroBioSed

2.1.1. Previous Efforts

HydroBioSed was originally developed by Moriarty et al. (2017) in the Regional Ocean Modeling System (ROMS) (Haidvogel et al., 2000, 2008; Shchepetkin & McWilliams, 2003, 2009) by coupling a water column biogeochemical model (Fennel et al., 2006) to a vertically resolved sediment transport (Warner et al., 2008) and seabed diagenetic model (Soetaert et al., 1996). The water column biogeochemical model (Fennel et al., 2006) used nitrogen as the major currency and included seven state variables including phytoplankton, zooplankton, nitrate, ammonium, dissolved oxygen, and small and large detritus. Additionally, HydroBioSed accounted for water column concentrations of oxygen demand units (ODU), described below, for consistency with the seabed diagenetic process.

In the seabed, HydroBioSed used the Community Sediment Transport Modeling System with an added diagenetic algorithm based on Soetaert et al. (1996). CSTMS was developed in ROMS for non-cohesive sediment transport and seabed evolution (Warner et al., 2008). The diagenetic component was added by Moriarty et al. (2017) based on the diagenetic model proposed by Soetaert et al. (1996). Concentrations of labile organic matter, semi-labile organic matter, nitrate, ammonium and dissolved oxygen were represented in the seabed. Following Soetaert et al. (1996), other reduced chemical species were represented by a single tracer, called ODU. Aerobic remineralization, denitrification and anaerobic remineralization were represented to account for particulate organic matter decomposition. For anaerobic remineralization, one single pathway with a user specified stoichiometric ratio between oxidant and particulate organic matter was used to characterize the dominating anaerobic process. The seabed was modeled using multiple layers with different resolution from top to bottom (from submillimeter to centimeter thick). For each sediment layer, the distribution of both particulate organic matter and solutes were resolved.

This coupling of the water column biogeochemical model with the sediment transport and seabed diagenetic model facilitated representation of material exchange between the seabed and water column in a process-based way. This led to a more realistic representation of the bottom boundary used by Fennel et al. (2006), in which benthic flux was parameterized as a function of particulate organic matter properties and environmental variables assuming instantaneous remineralization of the deposited particulate organic matter. In HydroBioSed, the benthic fluxes were calculated for each baroclinic time step and applied to the bottommost (for water) or topmost (for seabed) grid cells. For particulate organic matter, the model accounted for seabed-water exchange through

YIN ET AL. 3 of 28

deposition and erosion. For the dissolved substances, in addition to the depositional/erosional flux, the diffusive flux between the sediment porewater and the overlying water column was also included.

A one-dimensional version of HydroBioSed was first implemented for the Rhone subaqueous delta to understand the effect of local resuspension on oxygen dynamics (Moriarty et al., 2017). Three-dimensional versions of HydroBioSed were then applied to the NGoM continental shelf to investigate the role of resuspension in regulating bottom water oxygen and nitrogen dynamics (Moriarty et al., 2018); and to the Chesapeake Bay to examine the role of resuspension on light attenuation, primary production and remineralization (Moriarty et al., 2021). Since then, the structure and algorithm of HydroBioSed was further updated and formally adapted to ROMS as released with the Coupled Ocean–Atmosphere–Wave–Sediment Transport (COAWST, see Warner et al., 2008, 2010) modeling system. Specifically, HydroBioSed was included in COAWST Version 3.8.

2.1.2. New Developments

This study focused on developing the model to account for the representation of the exchange of DIC and TAlk between the seabed and the water column. Specifically, we (a) implemented a version of the biogeochemical model that includes carbon dynamics in the water column (Fennel et al., 2008, 2013); (b) added DIC and TAlk to the seabed diagenetic model; (c) improved representation of anaerobic remineralization in the seabed by including manganese- and iron-oxides reduction, and sulfate reduction, which is believed to have a major impact on the benthic TAlk flux (Krumins et al., 2013); and (d) modified the representation of particulate organic matter to allow for unlimited classes of them with different remineralization rates in both water column and seabed. Additionally, the revised model was recalibrated based on recent observations of water column and seabed geochemistry from the NGoM.

2.2. Introduction to Model Processes

Figure 1 shows processes represented in HydroBioSed. In the water column, the temporal evolution of particulate and solute concentrations is calculated as the result of advection, diffusion and local biogeochemical reactions. Within the seabed, a sequence of idealized reactions is used to represent the major early diagenetic pathways. The mixing of particulate and dissolved materials in sediment is represented as a one-dimensional (vertical) diffusive process (bio-diffusion). At the seabed-water interface, the model considers the particle and solute exchange through deposition, erosion, and diffusion. At each baroclinic timestep, the biogeochemical reactions in the water column, net deposition/erosion and diffusion at the interface, bio-diffusion and diagenetic reactions within the seabed, and physical advection and diffusion in the water column are calculated in sequence. Table 1 shows the changes in DIC and TAlk associated with each of the reactions represented in HydroBioSed. The water column biogeochemical reactions follow Fennel et al. (2008, 2013) while the diagenetic reactions are from Soetaert et al. (1996).

2.2.1. Water Column Biogeochemical Processes

As shown in Figure 1, the major state variables included are phytoplankton (Phy), zooplankton (Zoo), nitrate (NO₃), ammonium (NH₄), DIC, dissolved oxygen (O₂), small detritus—nitrogen (SDetN), large detritus—carbon (LdetC), ODU, and total alkalinity (TAlk). The reactions represented in the model are shown in Figure 1 (top right). The time rates of change for the concentrations of solutes (mmol/m³) in the water column are calculated following Equations 1–6, with terms described in Table 2. New additions to HydroBioSed, that is, the equations of state for DIC and TAlk, are highlighted using bold print (Equations 4–5). These equations allow us to account for carbon cycling in the water column, and were based on Fennel et al. (2008, 2013), who has incorporated them into ROMS. Note that more detailed versions of the equations are provided in the supplementary material.

$$\frac{\partial NO_3}{\partial t} = -Phy_{NO3} + WNitri_{NO3} + Dep_{NO3} + Ero_{NO3} + SWDiff_{NO3} + Adv_{NO3} + WDiff_{NO3}$$
 (1)

$$\frac{\partial NH_4}{\partial t} = -Phy_{NH4} + Zoo_{NH4} - WNitri_{NH4} + Rem_{LDN,NH4} + Rem_{SDN,NH4} + WRem_{Mi,NH4} + WRem_{Ma,NH4} + Dep_{NH4} + Ero_{NH4} + SWDiff_{NH4} + Adv_{NH4} + WDiff_{NH4}$$
 (2)

YIN ET AL. 4 of 28

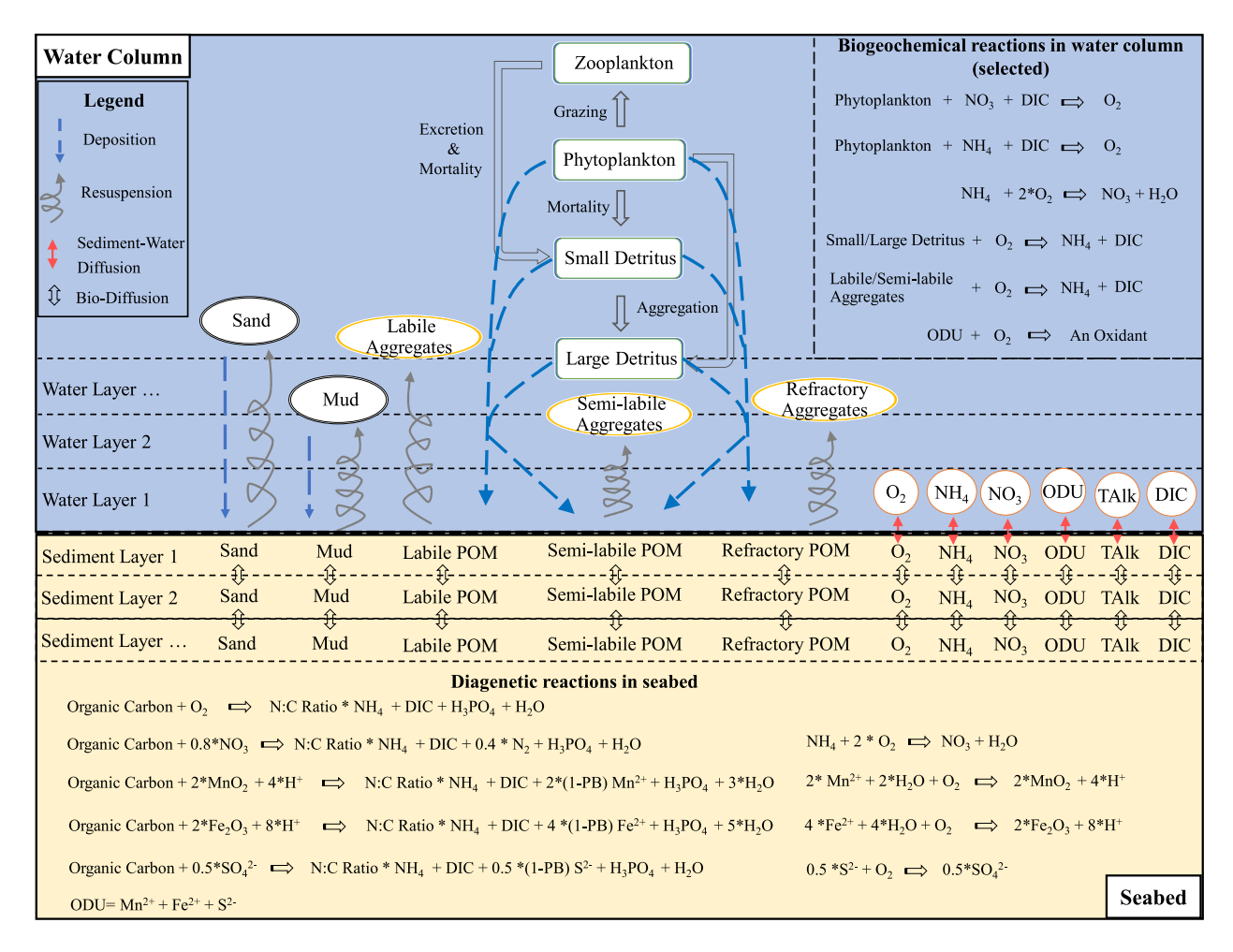


Figure 1. Schematic representation of the modeled processes. In the water column, the model accounts for the physical transport as well as the biogeochemical reactions of organic particles (outlined in black), biogeochemical solutes (outlined in yellow) and other state variables (outlined in green), and for suspended sediment transport (outlined in black). Within the seabed, geochemistry is modeled using a series of diagenetic reactions. The bio-diffusion of both solutes and particles between seabed layers are also represented as double arrows. At the seabed-water interface, the particulates and solutes are exchanged through diffusion, deposition, and erosion.

$$\begin{split} \frac{\partial O_2}{\partial t} &= Phy_{O_2} - Zoo_{O_2} - WNitri_{O_2} - Rem_{LDN,O_2} - Rem_{SDN,O_2} - WRem_{Mi,O_2} - WRem_{Ma,O_2} - WOxid_{ODU} \\ &\quad + AirSea_{O_2} + Dep_{O_2} + Ero_{O_2} + SWDiff_{O_2} + Adv_{O_2} + WDiff_{O_2} \end{split} \tag{3}$$

$$\frac{\partial DIC}{\partial t} = -Phy_{DIC} + Zoo_{DIC} + Rem_{LDC,DIC} + Rem_{SDC,DIC} + WRem_{Mi,DIC} + WRem_{Ma,DIC} + AirSea_{DIC} + Dep_{DIC} + Ero_{DIC} + SWDiff_{DIC} + Adv_{DIC} + WDiff_{DIC}$$
(4)

$$\frac{\partial TAlk}{\partial t} = Phy_{NO3} - Phy_{NH4} + Zoo_{NH4} - WNitri_{NH4} - WNitri_{NO3} + Rem_{LDN,NH4} + Rem_{SDN,NH4} + WRem_{Mi,NH4} + WRem_{Ma,NH4} + Dep_{TAlk} + Ero_{TAlk} + SWDiff_{TAlk} + Adv_{TAlk} + WDiff_{TAlk}$$
 (5)

$$\frac{\partial ODU}{\partial t} = -WOxid_{ODU} + Dep_{ODU} + Ero_{ODU} + SWDiff_{ODU} + Adv_{ODU} + WDiff_{ODU}$$
 (6)

2.2.2. Seabed Geochemical Processes

The calculation of the particulate organic matter content in each sediment layer $(POM_i, \text{kg/m}^2)$ follows Equation 7, and accounts for aerobic remineralization $(OxicM_i)$, nitrification $(SDeni_i)$ and anaerobic remineralization

YIN ET AL. 5 of 28

Table 1
Reactions Implemented in HydroBioSed and the Related Changes in TAlk and DIC

Process	$\Delta TAlk$	ΔDIC	Source
Water column			
Phytoplankton + DIC + $NO_3 \rightarrow O_2$	1	-6.625	Fennel et al. (2008, 2013)
Phytoplankton + DIC + $NH_4 \rightarrow O_2$	-1	-6.625	
$NH_4 + O_2 \rightarrow NO_3 + H_2O$	-2	0	
Small/Large Detritus + $O_2 \rightarrow DIC + NH_4$	1	6.625	
Labile/Semi-labile Aggregates + $O_2 \rightarrow DIC + NH_4$	1	6.625	
Seabed			
$POM + O_2 \rightarrow NH_4 + DIC + H_3PO_4 + H_2O$	0.11	1	Soetaert et al. (1996)
$POM + NO_3 \rightarrow NH_4 + DIC + N_2 + H_3PO_4 + H_2O$	0.94	1	
$POM + MnO2 + H+ \rightarrow NH4 + DIC + Mn2+ + H3PO4 + H2O$	4.14	1	
$POM + Fe_2O_3 + H^+ \rightarrow NH_4 + DIC + Fe^{2+} + H_3PO_4 + H_2O$	8.14	1	
$POM + SO_4^{2-} \rightarrow NH_4 + DIC + S^{2-} + H_3PO_4 + H_2O$	1.14	1	
$NH_4 + O_2 \rightarrow NO_3 + H_2O$	-2	0	
$\mathrm{Mn^{2+}} + \mathrm{H_2O} + \mathrm{O_2} \rightarrow \mathrm{MnO_2} + \mathrm{H^+}$	-2	0	
$Fe^{2+} + H_2O + O_2 \rightarrow Fe_2O_3 + H^+$	-2	0	
$S^{2-} + O_2 \rightarrow SO_4^{\ 2-}$	-2	0	

 $(AnoxicM_i)$ (Equations 8–11) (Moriarty et al., 2017, 2018, 2021). New additions to HydroBioSed are highlighted using bold print (Equation 12) and led to a more realistic representation of anaerobic remineralization in the seabed. Instead of assuming a dominant anaerobic pathway as in the previous versions of HydroBioSed, the revised model used two coefficients (f_{Mn} and f_{Fe}) to partition the $AnoxicM_i$ into three classes: manganese-oxides reduction $AnoxicM_{Mn,i}$, iron-oxides reduction $AnoxicM_{Fe,i}$ and sulfate reduction $AnoxicM_{SO4,i}$. These two

 Table 2

 Terms Used in the Water Column Biogeochemical Model (Equations 1–6)

Terms	Description		
Phy _i	The solute change induced by phytoplankton growth (uptake for NO ₃ , NH ₄ and DIC; production for O ₂ ; mmol/m ³ s).		
Zoo_i	The solute change induced by zooplankton excretion (consumption for ${\rm O_2}$; production for NH $_4$ and DIC; mmol/m 3 s).		
$WNitri_i$	The solute change induced by water column nitrification (consumption for NH_4 and O_2 ; production for NO_3 ; mmol/m ³ s).		
$Rem_{LDN,i}, Rem_{SDN,i}, WRem_{Mi,i}, WRem_{Ma,i}$	The O_2 consumption and NH_4 production from LdetN, SdetN, labile (MiOM) and semi-labile (MaOM) particulate organic matter remineralization in the water column, respectively (mmol/m ³ s).		
$Rem_{LDC,DIC}, Rem_{SDC,DIC}, WRem_{Mi,DIC}, WRem_{Ma,DIC}$	The DIC production from LdetC and SdetC, labile (MiOM) and semi-labile (MaOM) particulate organic matter remineralization in the water column, respectively (mmol/m³ s).		
$WOxid_{ODU}$	ODU oxidation in the water column (mmol/m ³ s).		
$AirSea_{DIC/O_2}$	Air-sea exchange of DIC and O ₂ (mmol/m ³ s).		
Dep_i , Ero_i	Depositional and erosional flux of particulate and solutes at the seabed-water interface (mmol/ \mbox{m}^3 s).		
$SWDiff_i$	Diffusive flux of solutes at the seabed-water interface (mmol/m ³ s).		
$Adv_i, WDiff_i$	Advection and diffusion in the water column (mmol/m ³ s).		

Note. 1) The class of solute or particulate is represented using index i; 2) The uptake of NO_3 and NH_4 cause decrease and increase of TAlk, respectively; 3) ODU oxidation causes O_2 consumption; 4) Air-sea exchange is only applied to the topmost water grid cell, 5) Dep_i , Ero_i , $SWDiff_i$ are only applied to the bottom-most water grid cell.

YIN ET AL. 6 of 28

coefficients (f_{Mn} and f_{Fe}) can be determined based on a modified Monod formulation limited by the concentrations of Mn(IV), Fe (III) and SO_4^{2-} when available (e.g., Morse & Eldridge, 2007; Van Cappellen & Wang, 1996), or through model calibration when those concentration values are not available. The description of each term in Equations 7–12 is detailed in Table 3. For Equations 8–10, following Soetaert et al. (1996), the decomposition rate of the particulate organic matter depends on the degradability of the organic matter (γ_i), the temperature (T) and the concentrations of the oxidants. Additionally, the presence of some oxidants (e.g., O_2) may inhibit other diagenetic pathways (e.g., denitrification and anaerobic remineralization). In addition to chemical processes, bio-diffusion ($BioDiff_i$), deposition of biological materials ($BDep_i$) and suspended particulate organic matter ($SDep_i$), as well as erosion (Ero_i) will affect the particulate organic matter content (POM_i), the calculation of which is detailed in Sections 2.2.3 and 2.2.4 below.

$$\frac{\partial POM_i}{\partial t} = -OxicM_i - Deni_i - AnoxicM_i + BioDiff_i + SDep_i + BDep_i + Ero_i \tag{7}$$

$$OxicM_i = \gamma_i * 3^{\frac{7-20.0}{10.0}} * POM_i * \frac{O2}{O2 + k_{O2}} * \frac{1}{\sum lim}$$
 (8)

$$Deni_{i} = \gamma_{i} * 3^{\frac{7-20.0}{10.0}} * POM_{i} * \left(\frac{NO3}{NO3 + k_{NO3}}\right) * \left(1 - \frac{O2}{O2 + k_{Doni}^{O2}}\right) * \frac{1}{\sum lim}$$
(9)

$$AnoxicM_i = \gamma_i * 3^{\frac{7-20.0}{10.0}} * POM_i * \left(1 - \frac{NO3}{NO3 + k_{Anoxio}^{NO3}}\right) * \left(1 - \frac{O2}{O2 + k_{Anoxio}^{O2}}\right) * \frac{1}{\sum lim}$$
(10)

$$\sum \lim \frac{O2}{O2 + k_{O2}} + \left(\frac{NO3}{NO3 + k_{NO3}}\right) * \left(1 - \frac{O2}{O2 + k_{Doris}^{O2}}\right) + \left(1 - \frac{NO3}{NO3 + k_{NO3}^{NO3}}\right) * \left(1 - \frac{O2}{O2 + k_{Doris}^{O2}}\right)$$
(11)

$$AnoxicM_{Mn,i} = f_{Mn} * AnoxicM_i,$$

$$AnoxicM_{Fe,i} = f_{Fe} * AnoxicM_i,$$

$$AnoxicM_{SO4,i} = (1 - f_{Mn} - f_{Fe}) * AnoxicM_i$$
(12)

Solute concentrations in the porewater in the seabed change in time based on the diagenetic reactions used (Figure 1; Equations 13–18). Note that the dissolved chemical species are in units of mmol/ m^2) in Equations 13–18, and Table 3 provides a description of each term. Processes that are new to this version of the model are in bold print (Equations 15–18). New additions include accounting for the contributions of various anaerobic remineralization pathways (i.e., manganese- and iron-oxides reduction, and sulfate reduction) in the formulas used for the calculations of O_2 (Equation 15) and ODU (Equation 16). In addition, the DIC and TAlk concentrations are calculated following Equation 17 and Equation 18 (Soetaert et al., 1996), respectively. Besides the diagenetic reactions, physical processes including deposition (Dep_i), erosion (Ero_i), bio-diffusion ($BioDiff_i$) and diffusion across the sediment-water interface ($SWDiff_i$) will also affect the porewater concentrations of solutes, the calculation of which is detailed in Sections 2.2.3–2.2.5 below. Descriptions of specific equations are given in the following paragraphs.

In Equation 13, the porewater concentration of NO₃ is influenced by both nitrification (1st right-hand term) and denitrification (2nd right-hand term). The contribution from nitrification depends on the nitrification rate ($\gamma_{S,Nitri}$), as well as the porewater concentrations of NH₄ and O₂. The limitation of O₂ on nitrification rate is represented using a half-saturation constant k_{Nitri}^{O2} . Similarly, in Equation 14, the porewater concentration of NH₄ is increased by denitrification (1st right-hand term) and decreased by nitrification (2nd right-hand term) and NH₄ absorption (3rd right-hand term).

In Equation 15, the porewater concentration of O_2 is decreased by the aerobic remineralization of particulate organic matter (1st right-hand term) and nitrification (2nd right-hand term). New additions account for the consumption of O_2 from reoxidation of different reduced chemical species (3rd right-hand term). The reoxidation of ODU is limited by the concentration of O_2 with a half-saturation constant k_{ODU}^{O2} . Reoxidation of 1 unit of Mn²⁺, Fe²⁺ and S²⁻ consumes 0.5, 0.25 and 2 units of O_2 , respectively.

YIN ET AL. 7 of 28

Table 3 *Terms/Parameters Used in the Seabed Diagenetic Model (Equations 7–19)*

Terms/Parameters	Description			
OxicM _i	Aerobic remineralization of particulate organic matter in seabed (kg/m ² s).			
Deni _i	Denitrification of particulate organic matter in seabed (kg/m ² s).			
$Anoxic M_i$	Anoxic remineralization of particulate organic matter in seabed (kg/m ² s).			
$\mathit{BioDiff}_i$	Bio-diffusion of particulate (kg/m ² s) or dissolved substance (mmol/m ² s) in seabed.			
$SWDiff_i$	Diffusive flux of dissolved substance (mmol/m ² s) across the seabed-water interface.			
$BDep_i$	Particulate organic matter deposition from the Phy, LdetN and SdetN (kg/ m^2 s).			
$SDep_i$	Particulate organic matter deposition from the suspended particulate organic matter in water column (kg/m² s).			
Ero_i	Particulate organic matter erosion (kg/m ² s).			
γ_i	Remineralization rate of particulate organic matter in seabed (1/day).			
$\gamma_{S,Nitri}$	Maximum nitrification rate in seabed (1/day).			
$\gamma_{S,ODU}$	Maximum oxidation rate of oxygen demand units in seabed (1/day).			
T	Temperature in the seabed (°C).			
k_{O2}	Half-saturation constant for O_2 limitation of aerobic remineralization in seabed (mmol/m ³).			
k_{NO3}	Half-saturation constant for NO ₃ limitation of denitrification in seabed (mmol/m ³).			
k_{Deni}^{O2}	Half-saturation constant for O ₂ limitation of denitrification in seabed (mmol/m ³).			
k_{Anoxic}^{O2}	Half-saturation constant for O_2 limitation of anoxic remineralization in seabed (mmol/m ³).			
k_{Anoxic}^{NO3}	Half-saturation constant for NO ₃ limitation of anoxic remineralization in seabed (mmol/m ³).			
P	Sediment porosity (dimensionless).			
NC_i	Nitrogen-Carbon ratio of particulate organic matter in seabed (dimensionless).			
PB	The proportion of ODU that is deposited as solid (dimensionless).			
f_{Mn}	The proportion of anaerobically remineralized particulate organic matter that can be attributed to manganese-oxides reduction $(0\sim1,$ dimensionless).			
f_{Fe}	The proportion of anaerobically remineralized particulate organic matter that can be attributed to iron oxidation $(0\sim1, \text{dimensionless})$.			
n	The total number of classes of particulate organic matter with larger than zero remineralization rate in seabed.			
S_i	Porewater concentration of the dissolved substance (mmol/m ³).			
z	Depth in seabed, which is positive downward with zero at the seabed- water interface (m).			
kg2mmolC	The ratio of particulate organic matter mass to mmol Carbon (mmol/kg)			
δ_{NH4}	The absorption coefficient of NH ₄ (dimensionless).			
$D_{b,i}$	The bio-diffusion coefficient of the dissolved substance (m ² /s).			

Note. The class of particulate organic matter or dissolved substance in seabed porewater is represented using index i.

YIN ET AL. 8 of 28



In Equation 16, the anaerobic remineralization of particulate organic matter (1st right-hand term) produces ODU, which is calculated as the total concentrations of Mn^{2+} , Fe^{2+} and S^{2-} . The remineralization of 1 unit of particulate organic carbon produces 2, 4 and 0.5 units of Mn^{2+} , Fe^{2+} and S^{2-} , respectively. Here, PB represents the proportion of the reduced chemical species that forms as a solid. Oxygen demand units can also be removed by the reoxidation process (2nd right-hand term).

In Equation 18, the contribution of organic matter respiration to TAlk production is considered through a series of remineralization pathways, wherein different stoichiometric ratios between the amount of organic matter decomposed and that of TAlk produced are used (Table 1). Specifically, the porewater concentration of TAlk is increased by aerobic remineralization (1st right-hand term), denitrification (2nd right-hand term), and anaerobic remineralization (3rd right-hand term). It is decreased by the reoxidation process (4th right-hand term), nitrification (5th right-hand term) and absorption of NH₄ (6th right-hand term). Note that the influence of the formation of the solid-phase species from ODU on TAlk is also considered in Equation 16. In general, reoxidation of 1 unit of ODU will result in the removal of 2 units of TAlk. Additionally, the denitrification of 1 unit of NO₃⁻ produces 1.18 units of TAlk and 0.19 unit of NH₄, while the nitrification of 1 unit of NO₃⁻ following the nitrification of the NH₄ will lead to a net gain of 0.8 unit in TAlk. The denitrification rate is limited by the porewater concentrations of nitrate and oxygen. The nitrification rate is limited by the porewater concentrations of nitrate and oxygen. The nitrification-nitrification reactions on TAlk depends on the relative concentrations of nitrate (the major factor), oxygen, and particulate organic matter in the model.

$$\frac{\partial NO_3}{\partial t} = \gamma_{S,Nitri} * NH4 * \frac{O2}{O2 + k_{Nitri}^{O2}} - 0.8 * \frac{1 - P}{P} * \left(\sum_{i=1}^n kg2mmolC * Deni_i\right) + Dep_{NO3} + Ero_{NO3} + SWDiff_{NO3} + BioDiff_{NO3}$$

$$(13)$$

$$\frac{\partial NH_4}{\partial t} = \frac{1 - P}{P} * \left(\sum_{i=1}^{n} kg2mmolC * NC_i * \gamma_i * 3^{\frac{7 - 200}{1000}} * POM_i \right) - \gamma_{S,Nitri} * NH4 * \frac{O2}{O2 + k_{Nitri}^{O2}} - \frac{\delta_{NH4}}{1 + \delta_{NH4}} * NH_4 + Dep_{NH4} + Ero_{NH4} + SWDiff_{NH4} + BioDiff_{NH4} \tag{14}$$

$$\frac{\partial O_2}{\partial t} = -\frac{1 - P}{P} * \left(\sum_{i=1}^{n} kg2mmolC * OxicM_i \right) - 2 * \gamma_{S,Nitri} * NH4 * \frac{O2}{O2 + k_{Nitri}^{O2}} - \gamma_{S,ODU} * ODU * \frac{O2}{O2 + k_{ODU}^{O2}} * \left[0.5 * f_{Mn} + 0.25 * f_{Fe} + 2 * \left(1 - f_{Mn} - f_{Fe} \right) \right] + Dep_{O2} + Ero_{O2} + SWDiff_{O2} + BioDiff_{O2}$$
(15)

$$\frac{\partial ODU}{\partial t} = (\mathbf{1} - PB) * \frac{\mathbf{1} - P}{P} * \left(\sum_{i=1}^{n} kg2mmolC * AnoxicM_{i} \right) * \left[2 * f_{Mn} + 4 * f_{Fe} + 0.5 * \left(\mathbf{1} - f_{Mn} - f_{Fe} \right) \right]$$

$$- \gamma_{S,ODU} * ODU * \frac{O2}{O2 + k_{ODU}^{O2}} + Dep_{ODU} + Ero_{ODU} + SWDiff_{ODU} + BioDiff_{ODU}$$

$$(16)$$

$$\frac{\partial DIC}{\partial t} = \frac{1 - P}{P} * \left(\sum_{i=1}^{n} kg 2mmolC * \gamma_i * 3^{\frac{T - 20.0}{10.0}} * POM_i \right) + Dep_{DIC} + Ero_{DIC} + SWDiff_{DIC} + BioDiff_{DIC}$$
(17)

$$\frac{\partial TAlk}{\partial t} = 0.11 * \frac{1 - P}{P} * \left(\sum_{i=1}^{n} kg2mmolC * OxicM_{i} \right) + 1.18 * 0.8 * \frac{1 - P}{P} * \left(\sum_{i=1}^{n} kg2mmolC * Deni_{i} \right) \\
+ \frac{1 - P}{P} * \left(\sum_{i=1}^{n} kg2mmolC * AnoxicM_{i} \right) * \left[\left(\frac{439}{106} \right) * f_{Mn} + \left(\frac{863}{106} \right) * f_{Fe} + \left(\frac{121}{106} \right) * \left(1 - f_{Mn} \right) \\
- f_{Fe} \right] - 2 * \gamma_{S,ODU} * ODU * \frac{O2}{O2 + k_{ODU}^{O2}} - 2 * \gamma_{S,Nitri} * NH4 * \frac{O2}{O2 + k_{Nitri}^{O2}} - \frac{\delta_{NH4}}{1 + \delta_{NH4}} * NH_{4} \\
+ Dep_{TAlk} + Ero_{TAlk} + SWDiff_{TAlk} + BioDiff_{TAlk} \tag{18}$$

YIN ET AL. 9 of 28

2.2.3. Bio-Diffusion in the Seabed

In the current version of HydroBioSed, the mixing of dissolved substances in sediment porewater by molecular diffusion and biological processes is represented as a vertical diffusive process following Sherwood et al. (2018) and Soetaert et al. (1996), in which non-local mixing is not represented:

$$\frac{\partial S_i}{\partial t} = \frac{\partial}{\partial z} \left(D_{b,i} * \frac{\partial S_i}{\partial z} \right) \tag{19}$$

where S_i is the porewater concentration of the dissolved substances i (mmol/m³); z (m) is the depth in the seabed, which is positive downward with zero at the seabed-water interface; $D_{b,i}$ is the user-specified bio-diffusion coefficient (m²/s) of tracer i. Values of $D_{b,i}$ are different for each solute.

2.2.4. Benthic Flux Induced by Resuspension

The net depositional/erosional flux of particulate organic matter $(kg/m^2 s)$ is calculated using Equation 20, which is similar to the one used for non-cohesive suspended sediment (Warner et al., 2008), following Moriarty et al. (2017). The description of each term is detailed in Table 4. This flux represents an exchange between the seabed and the water column; for example, during deposition it will provide a source to the top-most layers of the seabed and an equivalent sink to the bottom-most layer of the water column.

 $BDep_i$ includes the deposition from phytoplankton (Phy), large detritus nitrogen (LDetN) and small detritus nitrogen (SDetN). $SDep_i$ $(w_i\frac{\partial C_i}{\partial s})$ represents the depositional flux from the particulate organic matter aggregates (Figure 1). The erosional flux is Ero_i $(\{...\})$. Following the formulation for sediment erosion from Warner et al. (2008), the POM erosional flux is calculated as the smaller value between the erosion based on bed shear stress $(max\Big[\Big(E_{0,i}*(1-P)*\Big(\frac{\tau_{yj}-\tau_{cri,i}}{\tau_{cri,i}}\Big),0\Big])$, and the amount of particulate organic matter that is available for erosion in surficial sediment $\Big(\frac{\min(mass_{activ,i}, mass_{top,i})}{\Delta t} + w_i\frac{\partial C_i}{\partial s}\Big)$.

$$Flux_{pom,i} = BDep_i + SDep_i - Ero_i$$

$$= f_i * \frac{1}{kg2mmolC} * CN_{Phy} * \left(w_{Phy} \frac{\partial Phy}{\partial s} + w_{LDetN} \frac{\partial LDetN}{\partial s} + w_{SDetN} \frac{\partial SDetN}{\partial s} \right) + w_i \frac{\partial C_i}{\partial s}$$

$$- min \left\{ max \left[\left(E_{0,i} * (1 - P) * \left(\frac{\tau_{sf} - \tau_{cri,i}}{\tau_{cri,i}} \right), 0 \right], \frac{\min(mass_{activ,i}, mass_{top,i})}{\Delta t} + w_i \frac{\partial C_i}{\partial s} \right] \right\}$$

$$(20)$$

Similarly, the net flux of dissolved substances (mmol/m² s) due to entrainment of porewater during resuspension is calculated following Equation 21. When net deposition occurs, it is assumed that porewater within the deposited layer of sediment has the same solute concentrations as the source water grid cell, and the solutes that are incorporated into the seabed are removed from the bottom water column grid cell. Similarly, this assumes that porewater within a layer that was eroded is added to the solutes within the bottom-most water grid cell.

 $Flux_{solute,i}$ is calculated by multiplying the thickness of the eroded or deposited sediment layer $\left(\frac{Flux_{pom}}{\rho_m^*(1-P)}\right)$, the sediment porosity (P) and the concentration of solutes in the source water $(S_i \text{ when } Flux_{pom} < 0, \text{ and } C_i \text{ when } Flux_{pom} > 0)$. The description of each term in Equation 21 is detailed in Table 4.

$$Flux_{solute,i} = \frac{Flux_{pom}}{\rho_m * (1 - P)} * P * C_i, \quad when \ Flux_{pom} > 0$$

$$Flux_{solute,i} = \frac{Flux_{pom}}{\rho_m * (1 - P)} * P * S_i, \quad when \ Flux_{pom} < 0$$

$$(21)$$

2.2.5. Diffusive Flux Across the Seabed-Water Interface (SWDiff)

The model additionally accounts for benthic fluxes of dissolved substances across the seabed–water interface as a diffusive flux (*SWDiff*, mmol/m² s). These fluxes are applied to the bottom-most grid cell in the water column and

YIN ET AL. 10 of 28

Table 4 *Terms/Parameters Used for Calculating Fluxes at the Seabed-Water Interface (Equations 20–24)*

Terms/Parameters	Description
$Flux_{pom,i}$	The net flux of particulate organic matter from deposition and erosion (kg/m ² s).
Flux _{solute,i}	The net flux of dissolved substance from deposition and erosion (mmol/m² s).
f_i	The partitioning coefficient of certain particulate organic matter.
W_{Phy}	The settling velocity of phytoplankton (m/d).
W_{LDetN}	The settling velocity of large detritus nitrogen (m/d).
W_{SDetN}	The settling velocity of small detritus nitrogen (m/d).
w_i	The settling velocity of particulate organic matter (mm/s).
C_i	The volumetric concentration of suspended particulate organic matter in the bottom water (kg/m³) or the volumetric concentration of solutes in the bottom water (mmol/m³).
$E_{0,i}$	The user specified erosion rate of the particulate organic matter in seabed (kg/m² s).
$ au_{sf}$	The wave and current induced bottom skin-friction stress (N/m ²).
$ au_{cri,i}$	The critical shear stress for erosion of particulate organic matter in seabed (N/m²).
mass _{activ,i}	The mass of particulate organic matter available in the active layer (kg/m²).
$mass_{top,i}$	The mass of particulate organic matter i available in the topmost layer of seabed (kg/m²).
ρ_m	The density of the particulate organic matter (kg/m ³).
$H_{S,top}$	The thickness of the topmost sediment layer (m).
$H_{W,bot}$	The thickness of the bottom most water layer (m).
$SWDiff_{Fic}$	The diffusive flux of dissolved substance calculated according to Fick's law at the seabed-water interface (mmol/ m^2 s).
$SWDiff_{Equi}$	The equilibrium flux of the dissolved substance at the seabed-water interface (mmol/m ² s).
D_{s-w}	The diffusive coefficient of the dissolved substance at the seabed-water interface (m ² /s).
CN_{Phy}	Carbon: Nitrogen ratio in phytoplankton (dimensionless).
S	Vertical sigma coordinate (dimensionless).
Δt	Baroclinic timestep of the numerical model (seconds).

Note. The class of particulate organic matter or the dissolved substance is represented using index i.

the topmost grid cell in the seabed and follow the convention of being positive upward and negative downward. Following Moriarty et al. (2017), the model provides two options for representing benthic fluxes due to diffusion across the seabed—water interface (Equations 22–24, terms defined in Table 4). The first option follows Soetaert et al. (1996) and assumes that the concentration in the top layer of the seabed equals that of the bottom-most water column layer. This assumption gives rise to the following fluxes ($SWDiff_{Equi}$, Equations 22 and 23). Here, the diffusive flux ($SWDiff_{Equi}$) is calculated as the product of the difference between the equilibrium concentration $\left(\frac{S_i * H_{S_imp} * P + C_i * H_{W_i,bot}}{H_{W_i,bot} + H_{S_i,op} * P}\right)$ and the initial solute concentration in the source water (S_i when diffusion is out of seabed, C_i when diffusion is into the seabed), and the water layer thickness ($H_{S,top} * P$ or $H_{W,bot}$) divided by the time step (Δt).

$$SWDiff_{Equi} = \frac{\left(S_i - \frac{S_i * H_{S,top} * P + C_i * H_{W,bot}}{H_{W,bot} + H_{S,top} * P}\right) * H_{S,top} * P}{\Delta t}$$
 when diffusion is out of seabed (22)

$$SWDiff_{Equi} = -\frac{\left(C_i - \frac{S_i * H_{S,top} * P + C_i * H_{W,bot}}{H_{W,bot} + H_{S,top} * P}\right) * H_{W,bot}}{\Delta t} \text{ when diffusion is into the seabed}$$
 (23)

Alternatively, these benthic fluxes can be calculated following Fick's law ($SWDiff_{Fic}$, Equation 24), which was used for this study. Here, D_{s-w} is the user specified diffusive coefficient (m^2/s) of the dissolved substance at the seabed-water column interface:

YIN ET AL. 11 of 28

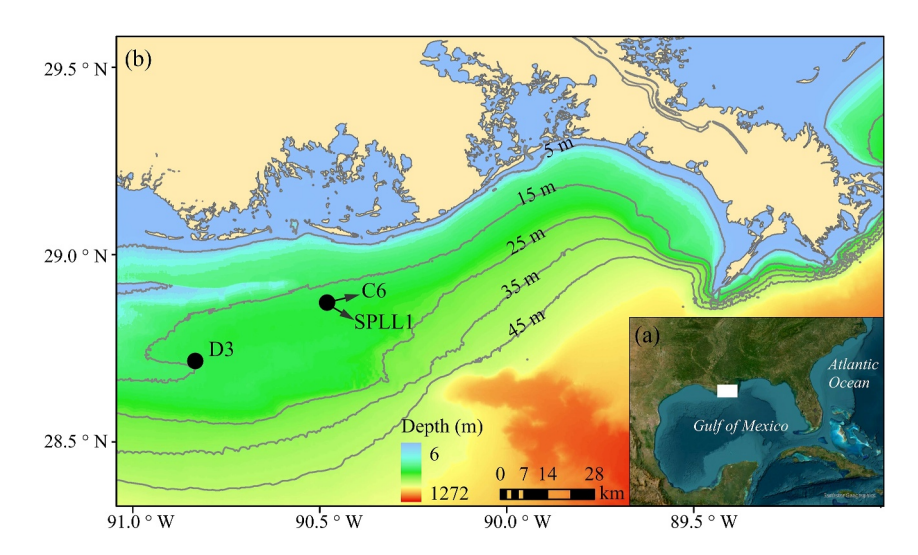


Figure 2. Maps showing (a) location of study area within the Gulf of Mexico, (b) continental shelf offshore of eastern Louisiana. Black circles represent locations of data collection sites used for model calibration and evaluation. Note that buoy station SPLL1 and site C6 are at the same location. Gray lines in panel (b) are bathymetric contours.

$$SWDiff_{Fic} = D_{s-w} * \frac{\partial C}{\partial z} = D_{s-w} * \frac{C_i - S_i}{H_{S,top}}$$
(24)

3. Model Calibration

The model described in Section 2.2 was applied in 1-D (vertical) to represent the NGoM hypoxic zone (Figure 2a) to showcase its capability to reproduce observed porewater profiles and benthic fluxes of major solutes.

3.1. Study Site and Model Calibration

A research cruise in August 2018 collected a data set that included dissolved oxygen concentration in the water column, sediment porosity, sediment porewater profiles, and benthic fluxes of major solutes (O₂, DIC, TAlk, NO₃ and NH₄). These data were used to parametrize, calibrate, and evaluate the model described in Section 2.2.

We calibrated a 1-D (vertical) version of HydroBioSed for sites C6 and D3 in the study area (Figure 2b; Table 5). The 1-D (vertical) model captures the vertical gradients in the seabed and the vertical fluxes across the seabedwater interface, which are larger in magnitude than their horizontal counterparts over the frequently hypoxic area in NGoM during summer (e.g., Justić et al., 2002; Rabalais et al., 1994). We assume that the observed benthic fluxes represented a semi-steady state condition as they were obtained during a fair weather period when bed shear stresses were too low to resuspend sediment. The benthic fluxes and near-surface porewater concentrations result mainly from the remineralization of recently deposited particulate organic matter with a high remineralization rate. The organic matter found deeper in the seabed is assumed to have had longer residence in the seabed and have a low remineralization rate. The goal of model calibration was to configure HydroBioSed so that it matched observations of porewater concentrations while using realistic representations of environmental conditions and physical processes. For the purpose of this paper, the water column was treated as the upper boundary condition for the seabed diagenetic model. The water column concentrations of phytoplankton and major solutes (O2, NO3, NH4, TAlk and DIC) were strongly nudged to steady values based on observations or literature reported values. In the seabed, sediment porosity was set as the depth-averaged value from observations. The parameters without observations (Table 5) were adjusted based on previous studies so that both simulated porewater concentration profiles and benthic flux matched observations. The model was run until a steady state condition was reached. Steady state was defined as the time beyond which the modeled benthic fluxes and porewater concentrations did not change. Unless otherwise stated, steady state porewater concentration(s) and steady state benthic flux (es) in this study represent the modeled porewater concentration(s) and benthic flux (es) of solutes after reaching steady state.

YIN ET AL. 12 of 28

19422466, 2024, 10, Downloaded from https://agupubs.onlinelibrary.wiley.com/doi/10.1029/2023MS004045, Wiley Online Library on [22/02/2025]. See the Terms and Conditions (https://onlinelibrary.wiley.com/terms-and-conditions) on Wiley Online Library for rules of use; OA articles are governed by the applicable Creative Commons License

 Table 5

 Model Implementation and Parameterization for Sites C6 and D3

			Va	lue		
Model parameter		Related equation	C6	D3	Source	
Water column biogeochemical	Water Depth (m)		20	18	Observation	
and transport parameters	Nitrate concentration in water column (NO ₃ , mmol/m ³)	Equation 1	4.631	1.689	Observation	
	Ammonium concentration in water column (NH_4 , mmol/m ³)	Equation 2	2.933	13.583	Observation	
	Oxygen concentration in water column $(O_2, \text{mmol/m}^3)$	Equation 3	53	35	Observation	
	DIC concentration in water column (DIC, mmol/m³)	Equation 4	2190	2220	Observation	
	TAlk concentration in water column (<i>TAlk</i> , mmol/m ³)	Equation 5	2306	2058	Observation	
	Phytoplankton concentration (<i>Phy</i> , mmol N/m ³)	Equation S1	0.8	0.8	Calibrated based on climatology values from Gomez et al. (2018	
	Small detritus nitrogen concentration (<i>SDetN</i> , mmol N/m³)	Equation S9	0.035	0.035	Calibrated based on model simulation from Moriarty	
	Large detritus nitrogen concentration (<i>LDetN</i> , mmol N/m³)	Equation S13	0.63	0.59	et al. (2018)	
	Settling (sinking) velocity of phytoplankton (ω_{Phy} , m/day)	Equation S1 and Equation 20	0.2	0.2	Calibrated based on values used Moriarty et al. (2018)	
	Settling (sinking) velocity of small detritus (ω_{SDetN} , m/day)	Equation S9 and Equation 20	0.2	0.2		
	Aggregation factor of phytoplankton and small detritus $(\tau, (\text{mmol N/m}^3)^{-1} \text{ day}^{-1})$	Equations S1 and S9	0.5	0.5		
	Settling (sinking) velocity of large detritus (ω_{LDetN} , m/day)	Equation S13 and Equation 20	9.0	9.0		
Seabed geochemical and transport parameters	Mass of semi-labile organic matter in the seabed $(POM, \times 10^{-6} \text{ kg/m}^2)$	Equations 7–10	3.0	3.0	Calibration	
	Labile organic matter remineralization rate (γ_i , 1/day)	Equations 7–10	0.1	0.1	Moriarty et al. (2018)	
	Semi-labile organic matter remineralization rate (γ_i , 1/day)	Equations 7–10	0.01	0.01	Calibration	
	Half-saturation constant for O_2 limitation of aerobic remineralization in seabed (k_{O2} , mmol/m ³)	Equation 8	1	1	Moriarty et al. (2017)	
	Half-saturation constant for NO_3 limitation of denitrification in seabed (k_{NO3} , mmol/m ³)	Equation 9	100	100	Calibrated based on values used Moriarty et al. (2017)	
Seabed geochemical and transport parameters	Half-saturation constant for O_2 limitation of denitrification in seabed (k_{Deni}^{O2} , mmol/m ³)	Equation 9	1	1	Moriarty et al. (2017)	
	Half-saturation constant for O_2 limitation of anoxic remineralization in seabed (k_{Anoxic}^{O2} , mmol/m ³)	Equation 10	1	1	Moriarty et al. (2017)	
	Half-saturation constant for NO $_3$ limitation of anoxic remineralization in seabed (k_{Anoxic}^{NO3} , mmol/m 3)	Equation 10	1	1	Calibrated based on values used Moriarty et al. (2017)	
	Maximum nitrification rate ($\gamma_{S,Nitri}$, 1/day)	Equation 13	10	10	Calibrated based on values used Moriarty et al. (2018)	
	Nitrogen-Carbon ratio of particulate organic matter in seabed (NC_i)	Equation 14	0.15	0.15	Moriarty et al. (2018)	
	Sediment Porosity (P, dimensionless)	Equations 13–18	0.79	0.53	Observation	
	Maximum oxidation rate of oxygen demand units $(\gamma_{S,ODU}, 1/\text{day})$	Equation 16	20	20	Moriarty et al. (2017)	
	The bio-diffusion coefficient of O_2 ($D_{b,i}$, $\times 10^{-10}$ m ² /s)	Equation 19	81.05	240.05	Calibrated with initial values base on Moriarty et al. (2018)	

YIN ET AL. 13 of 28

Table 5
Continued

	Value				
Model parameter		Related equation	C6	D3	Source
	The bio-diffusion coefficient of NH ₄ ($D_{b,i}$, $\times 10^{-10}$ m ² /s)		6.0	20.0	
	The bio-diffusion coefficient of ODU ($D_{b,i}$, $\times 10^{-10}$ m ² /s)		9.745	9.745	
	The bio-diffusion coefficient of NO ₃ ($D_{b,i}$, $\times 10^{-10}$ m ² /s)		9.780	4.90	
	The bio-diffusion coefficient of DIC ($D_{b,i}$, $\times 10^{-10}$ m ² /s)		4.807	20.00	Calibrated based on Hülse et al. (2018)
	The bio-diffusion coefficient of TAlk ($D_{b,i}$, $\times 10^{-10}$ m ² /s)		1.60	6.70	
	The bio-diffusion coefficient of sediment in seabed $(D_{b,i}, \times 10^{-10} \text{ m}^2/\text{s})$		2.785	2.785	Calibrated with initial values based on Moriarty et al. (2018)
Seabed-water interface	Partitioning of labile organic matter (f_i)	Equation 20	0.7	0.95	Calibration
parameters	Partitioning of refractory matter (f_i)	Equation 20	0.3	0.05	Calibration
	The diffusive coefficient of the solutes at the seabed- water interface $(D_{s-w}, \times 10^{-6} \text{ m}^2/\text{s})$	Equation 22	7.80	7.80	Calibrated based on Berelson et al. (2019)

3.2. Model-Data Comparison for the Calibration Runs

Figures 3 and 4 compare the modeled (black line) steady state porewater concentrations of five solutes under fair weather conditions against the measurements (blue dots) for the top 2–10 cm at site C6 and D3, respectively. In general, the modeled steady state porewater concentration profiles of major solutes match well with the measurements at both sites. For site C6, as shown in the observations and reproduced by the model, the penetration of O2 into the seabed is limited to the top ~3 mm (Figure 3a). The O2 porewater concentration decreases from ~53 mmol/m³ at the seabed—water interface to be less than 1 mmol/m³ at ~3 mm deep in the seabed. Due to the relatively high porewater concentration of O2 within the oxic layer (i.e., within ~3 mm from the sediment surface), aerobic respiration dominates the remineralization of the newly deposited labile materials while nitrification also occurs. As a result, porewater concentrations of NO3, NH4, DIC and TAlk exhibit sharp increases within the oxic layer (Figures 3b–3e), which is also reported by Berelson et al. (2019). As the depth increases, O2 quickly depletes, as does the amount of newly deposited labile organic material. Below the oxic layer, NO3 is used as the electron acceptor for the remineralization of particulate organic matter. Therefore, NO3 concentrations decrease below the surface layer (Figure 3b). In the deeper layers (i.e., deeper than ~1 cm from the sediment surface), anaerobic respiration dominates the decomposition, and the available organic matter has a low remineralization rate. This results in the gradual increase of NH4, DIC and TAlk concentrations there (Figures 3c–3e).

The sediment geochemistry at site D3 (Figure 4) shows similar behavior to that at site C6. Due to the low bottom water concentration of O_2 (35 mmol/m³) at site D3, the oxygen penetration depth is less than 2 mm (Figure 4a). Within the oxic layer (i.e., within \sim 2 mm from the sediment surface), aerobic remineralization dominates the decomposition of the labile materials, resulting in sharp increases in porewater concentrations of NO_3 , NH_4 , DIC and TAlk (Figures 4b–4e). Following the depletion of the O_2 , denitrification and anaerobic respiration rates increase and lead to the gradual decrease in the porewater concentration of NO_3 and gradual increase in the concentrations of NH_4 , DIC and TAlk (Figures 4c–4e).

In spite of the overall good performance of the model in simulating the porewater concentration-depth profiles, there are differences between simulations and observations. These differences could be attributed to (a) uncertainty in observations such as the NO₃ measurements below 5 cm; (b) uncertainty in model parameters such as the particulate organic matter properties (e.g., mass, vertical distribution, or remineralization rates) that can possibly cause overestimation of the anaerobic reaction intensity and underestimation of the NO₃ concentration in the upper 5 cm of the seabed; and (c) model limitations in representation of physical processes and chemical reactions. For instance, the model's underrepresentation of the possible non-local process that might be responsible

YIN ET AL. 14 of 28

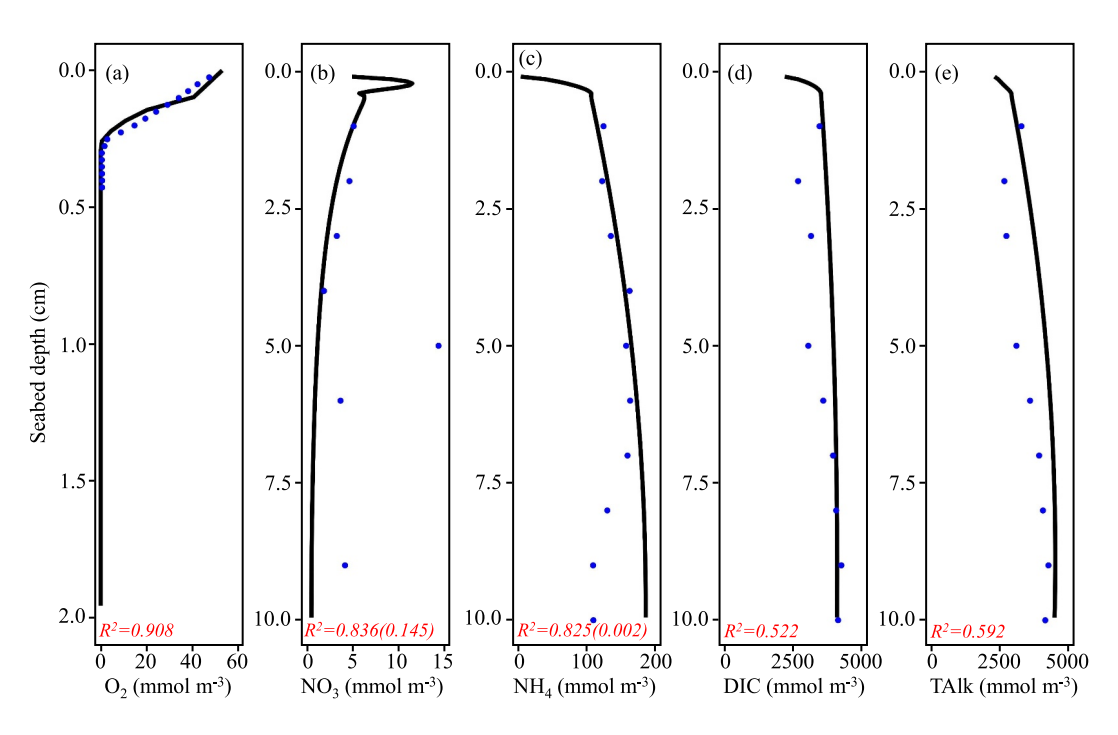


Figure 3. Sediment geochemistry for Site C6. Observed (blue dots) and simulated (black lines) porewater concentration of (a) O_2 , (b) NO_3 , (c) NH_4 , (d) DIC and (e) TAlk. The R^2 coefficients are also shown. In panels (b, c), the R^2 coefficients outside of the parentheses are calculated based on sediment geochemistry data from 0 to 5 cm and 0–7.5 cm, respectively. The R^2 coefficients in the parentheses are calculated based on all sediment geochemistry data. The location of the site is shown in Figure 2b. The observed data were collected in August 2018. Note difference in vertical scales between (a) and other panels.

for the decrease of NH_4 porewater concentration below 7.5 cm in the seabed (Cowie & Woulds, 2011) could explain the model-data difference shown in Figure 3c. Such model-data difference is also reported by Morse and Eldridge (2007). Model limitations are further discussed in Section 5.3.

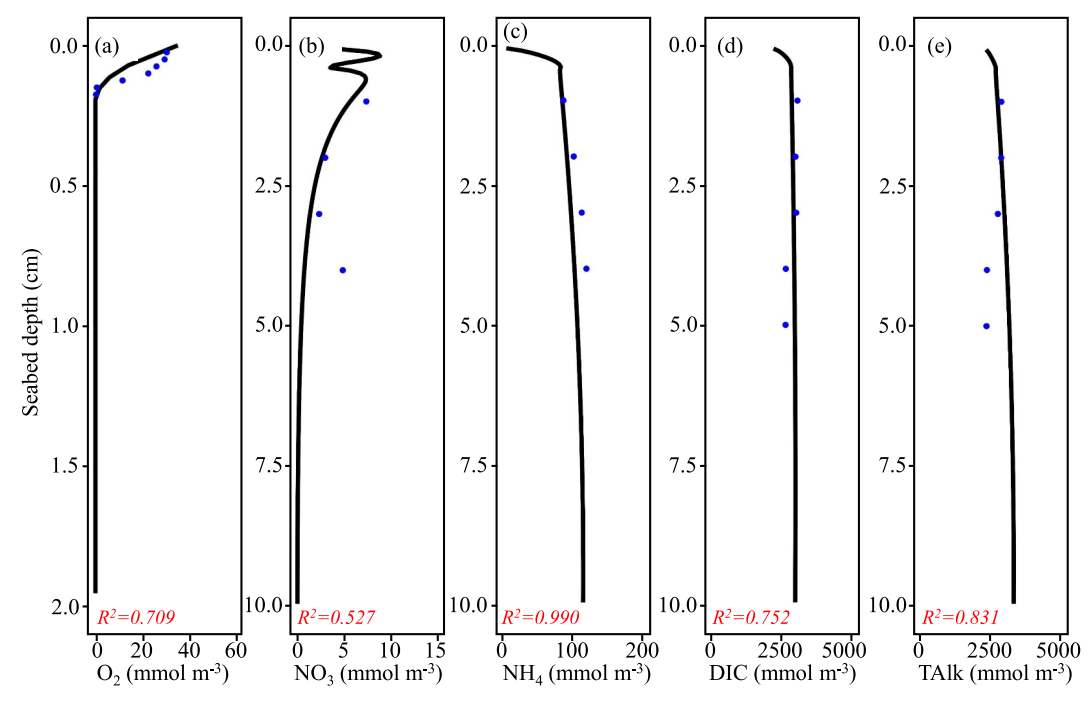


Figure 4. Same as Figure 3 but for site D3. Note difference in vertical scales between (a) and other panels.

YIN ET AL. 15 of 28

Table 6 *Modeled and Observed Benthic Fluxes* (m^2/d) *at Sites C6 and D3*

Site	Solute	Simulation	Observation
C6	DIC	27.905	27.365
	O_2	-25.039	-24.791
	TAlk	2.132	1.9–74.1
	NO_3	0.431	-1.82 - 0.26
	$\mathrm{NH_4}$	3.116	0–7.2
D3	DIC	34.755	35.157
	O_2	-23.514	-28.237
	TAlk	4.118	1.9–74.1
	NO_3	0.124	-1.82 - 0.26
	$\mathrm{NH_4}$	4.433	0.005-7.16

Note. (1) Positive values indicate flux out of the seabed while negative values indicate flux into the seabed; (2) TAlk, NO3 and NH4 observations are from Berelson et al. (2019).

Table 6 summarizes the modeled and observed benthic fluxes of major solutes at site C6 and D3. Positive fluxes indicate the release of solutes from the seabed to the water column while negative values indicate the seabed absorbed the fluxes. At both sites, the model satisfactorily reproduced both the direction and magnitude of benthic DIC and O_2 fluxes. The magnitude of the O_2 fluxes is only slightly smaller than the DIC fluxes, which implies that aerobic remineralization dominated organic matter decomposition on the seabed. Thus, TAlk fluxes are much smaller than those of DIC. Observations are not available for TAlk, NO_3 and NH_4 fluxes, but model simulations are within the ranges of previous reported values (Berelson et al., 2019).

Our modeled values of TAlk fluxes are on the lower side of those reported in Berelson et al. (2019). Meanwhile, the simulated DIC/TAlk ratios (8.4 at Site D3, 13.1 at Site C6) are generally larger than the observed values (larger than 1 but smaller than 1.7) from Berelson et al. (2019). There might be two reasons that could cause this difference. First and the major one, the dominant pathways for particulate organic matter decomposition were likely different in our study from during some of the conditions reported in Berelson et al. (2019). In our study, the magnitude of benthic oxygen flux is smaller

than but close to that for benthic DIC flux (Table). Thus, for the modeled conditions large proportions of particulate organic matter can be decomposed through the aerobic pathway rather than the anaerobic pathways, which normally results in a high DIC/TAlk ratio and relatively low TAlk flux. In Berelson et al. (2019), benthic oxygen fluxes were much smaller than the benthic DIC fluxes. In this case, the anaerobic pathways should dominate the decomposition of the particulate organic matter compared to the aerobic pathway, which generally results in relatively lower DIC/TAlk ratio and higher TAlk flux. Second, our model didn't capture some of ancillary processes such as biogenic silica dissolution and anaerobic oxidation of methane. This may also result in underestimation of benthic TAlk flux and overestimation of the DIC/TAlk ratio.

4. Sensitivity Tests

4.1. Configurations of Sensitivity Experiments

Following calibration of the model, a series of sensitivity experiments were conducted to gain insight on which environmental factors most impacted the benthic fluxes of DIC and TAlk during fair weather periods. The setup of the sensitivity experiments is shown in Table 7. Same as the calibration runs, the model was run until a steady state condition was reached. For the sensitivity tests, the range of parameter values were adjusted based on either observations (i.e., sediment porosity), or previous research (i.e., anerobic oxidation; Devereux et al., 2015). For the parameters whose ranges were less constrained by observations, the values of parameters were adjusted following similar studies (Moriarty et al., 2017; Morse & Eldridge, 2007).

4.2. Results of Sensitivity Tests

The benthic flux (Figure 5a) and porewater concentration of O_2 (Figures 5b and 5c) were most sensitive to labile material input, the bio-diffusive coefficient and sediment porosity. Increasing the labile material input enhanced the aerobic respiration rates in the surface sediment layer due to the increased availability of labile material. This led to an increase in benthic O_2 flux into the seabed (Figure 5a) and decrease in O_2 porewater concentration and penetration depth (Figure 5b). In addition, increasing the bio-diffusive coefficient of O_2 (Figure 5b) and sediment porosity (Figure 5c) increased the penetration depth and porewater concentration of O_2 , resulting in higher SOC (Figure 5a). Moreover, the anaerobic pathway (experiment suite "Apar" in Table 7) and bio-diffusive coefficient of sediment (experiment suite "BDSed" in Table 7) also influenced O_2 , although to a lesser degree. Anaerobic respiration influenced O_2 porewater concentration (Figure 5d) and benthic flux (Figure 5a) through reoxidation of the reduced species. The change of bio-diffusive coefficient of sediment also modified the vertical distribution of particulate organic matter, which changed the remineralization rate with depth, leading to changes in both porewater concentration (Figure 5c) and benthic flux of solutes (Figure 5a).

Benthic DIC flux only showed sensitivity to the labile material input (Figure 6a), which is reasonable considering the dominant control of particulate organic matter remineralization on DIC production. The profile of porewater

YIN ET AL. 16 of 28

 Table 7

 Setup of the Sensitivity Experiments

	Parameter tested	Related equation	Parameter values			
Exp. Suite			Sensitivity experiment	Calibration run		
Lab	Labile material partition coefficient (f_i)	Equation 20	Lab1:0.5	0.7		
			Lab2:0.6			
			Lab3:0.8			
			Lab4:0.9			
SP	Sediment Porosity (P)	Equations 13–18	SP1:0.49	0.79		
			SP2:0.59			
			SP3:0.69			
			SP4:0.89			
LRXN	Labile material remineralization Rate (γ_i , 1/day)	Equations 7–10	LRXN1:0.05	0.1		
			LRXN2:0.15			
Apar	Partition coefficient for Mn oxidation (FMN, f_{Mn})	Equation 12	Apar1: $FMN = 0.1$, $FFE = 0.1$	FMN = 0, FFE = 0		
	Partition coefficient for Fe oxidation (FFE, f_{Fe})					
	Partition coefficient for SO_4 oxidation $(1-f_{Mn}-f_{Fe})$					
			Apar2: FMN = 0.2 , FFE = 0.2			
			Apar3: FMN = 0.3 , FFE = 0.3			
BDSed	Bio-diffusive coefficient of sediment $(D_{b,i}, m^2/s)$	Equation 19	BDSed1:1.393 \times 10 ⁻¹⁰	2.785×10^{-10}		
			BDSed2:5.570 \times 10 ⁻¹⁰			
BDO2	Bio-diffusive coefficient of $O_2(D_{b,i}, m^2/s)$		BDO21: 40.53×10^{-10}	81.05×10^{-10}		
			BDO22: 162.1×10^{-10}			
BDTIC	Bio-diffusive coefficient of DIC $(D_{b,i}, \text{ m}^2/\text{s})$		BDTIC1: 2.404×10^{-10}	4.807×10^{-10}		
			BDTIC2: 9.614×10^{-10}			
BDTAlk	Bio-diffusive coefficient of TAlk $(D_{b,i}, (m^2/s))$		BDTAlk1: 0.8×10^{-10}	1.60×10^{-10}		
			BDTAlk2: 3.2×10^{-10}			
BDNH3	Bio-diffusive coefficient of NH_4 ($D_{b,i}$, m^2/s)		BDNH31: 3.0×10^{-10}	6.0×10^{-10}		
			BDNH32: 12.0×10^{-10}			
BDNO3	Bio-diffusive coefficient of NO ₃ ($D_{b,i}$, m ² /s)		BDNO31:4.39 \times 10 ⁻¹⁰	9.78×10^{-10}		
			BDNO32: 19.56×10^{-10}			
SWD	Diffusive coefficient at the seabed-water interface (D_{s-w} , m ² /s)	Equation 22	SWD1:3.54 \times 10 ⁻⁶	7.08×10^{-6}		
	, 3-w/ /	•	SWD2:14.16 \times 10 ⁻⁶			

DIC concentration was sensitive to labile material input, bio-diffusive coefficient of DIC, and sediment porosity (Figure 6b). The latter two influenced the DIC porewater concentration through their influence on bio-diffusion and effective volume of porewater, respectively.

TAlk exhibited the largest sensitivity to the adjusted parameters among the three solutes compared (Figure 7). Benthic TAlk flux was sensitive to labile material input, the anaerobic remineralization pathway, sediment porosity, and the bio-diffusive coefficient of O_2 (Figure 7a). Porewater concentration of TAlk was sensitive to labile material input, the anaerobic remineralization pathway, sediment porosity, the bio-diffusive coefficient of O_2 , TAlk, and particulate organic matter (Figures 7b and 7c). Like O_2 and DIC, an increase of labile organic material increased both the benthic flux and porewater concentration of TAlk by enhancing the remineralization intensity. In contrast, an increased bio-diffusive coefficient of O_2 or sediment porosity increased porewater oxygen concentration, which caused a decrease in benthic TAlk flux and porewater concentration. The reason was that increased oxygen concentrations enhanced reoxidation of reduced species, which suppressed the effects of anaerobic remineralization in increasing TAlk by releasing H⁺ (Canfield et al., 1993). In addition, higher contributions of manganese- and iron-oxides reduction to the anaerobic remineralization caused a sharp increase in

YIN ET AL. 17 of 28

19422466, 2024, 10, Downloaded from https://agupubs. online library.wiley.com/doi/10.1029/2023MS04045, Wiley Online Library on [22/02/2023]. See the Terms and Conditions (https://onlinelibrary.wiley.com/terms-and-conditions) on Wiley Online Library for rules of use; OA articles are governed by the applicable Creative Creative Creative Conditions (https://onlinelibrary.wiley.com/terms-and-conditions) on Wiley Online Library for rules of use; OA articles are governed by the applicable Creative Creative Conditions (https://onlinelibrary.wiley.com/terms-and-conditions) on Wiley Online Library for rules of use; OA articles are governed by the applicable Creative Creative Conditions (https://onlinelibrary.wiley.com/terms-and-conditions) on Wiley Online Library for rules of use; OA articles are governed by the applicable Creative Conditions (https://onlinelibrary.wiley.com/terms-and-conditions) on Wiley Online Library for rules of use; OA articles are governed by the applicable Creative Conditions (https://onlinelibrary.wiley.com/terms-and-conditions) on Wiley Online Library for rules of use; OA articles are governed by the applicable Creative Conditions (https://onlinelibrary.wiley.com/terms-and-conditions) on Wiley Online Library for rules of use; OA articles are governed by the applicable Creative Conditions (https://onlinelibrary.wiley.com/terms-and-conditions) on Wiley Online Library for rules of use; OA articles are governed by the applicable Conditions (https://onlinelibrary.wiley.com/terms-and-conditions) on Wiley Online Library for rules of use; OA articles are governed by the applicable Creative Conditions (https://onlinelibrary.wiley.com/terms-and-conditions) on Wiley Online Library for rules of use; OA articles are governed by the applicable Conditions (https://onlinelibrary.wiley.com/terms-and-conditions) on Wiley Online Library for rules of use; OA articles are governed by the applicable Conditions (https://onlinelibrary.wiley.com/terms-and-conditions) on Wiley Online Library for the applicable Condition

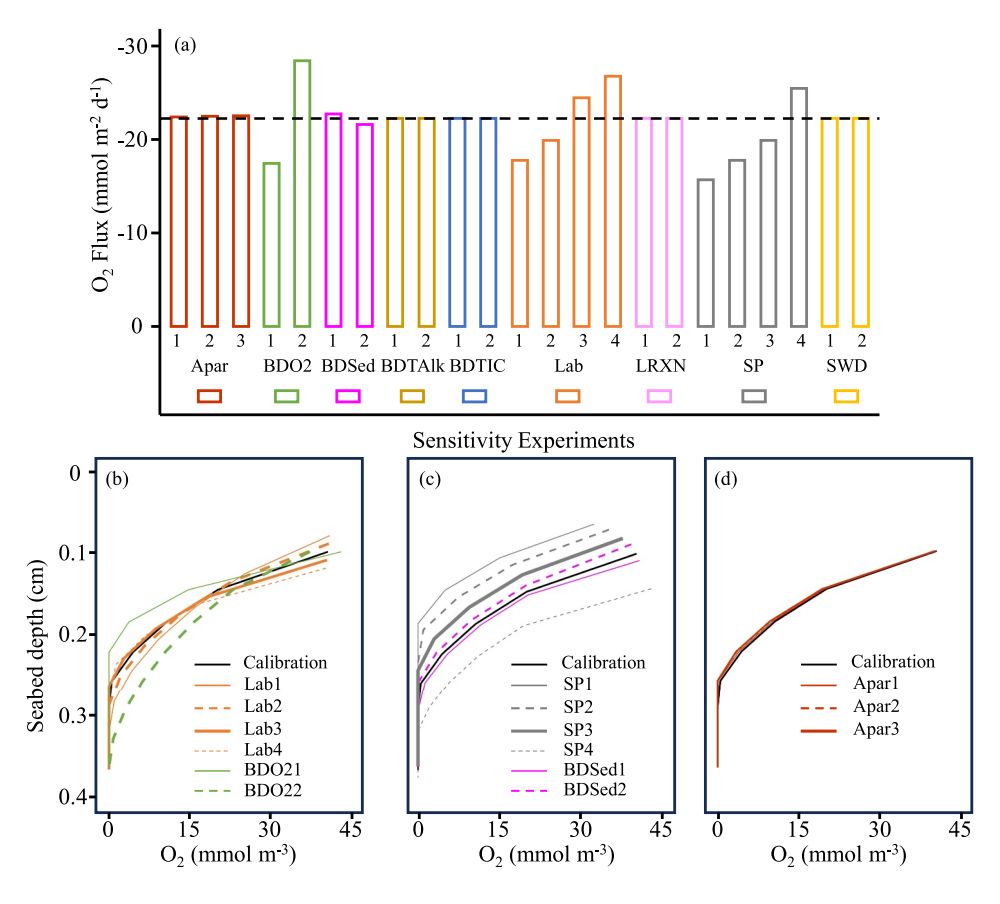


Figure 5. (a) Modeled benthic fluxes of O_2 for each sensitivity experiment listed in Table 7. The black dashed line is the modeled benthic flux of O_2 from the calibration run. (b-d) Modeled porewater concentrations of O_2 . Only results from experimental suites for which the modeled porewater concentrations were sensitive to the adjusted parameters are shown. The solid black line represents the porewater concentrations from the calibration run. In all panels the results for the various experimental suites listed in Table 7 are in distinct colors.

benthic TAlk flux (Figure 7a) and porewater concentration (Figure 7b). This was because manganese- and iron-oxides reduction increases TAlk at a faster rate than sulfate reduction. As seen for DIC, the bio-diffusive coefficient of TAlk affected the TAlk porewater concentration (Figure 7b), but not its benthic flux (Figure 7a).

Next, the DIC/TAlk ratio of benthic flux was calculated for each of the sensitivity experiments (Figure 8). Reflecting the sensitivity of TAlk, the DIC/TAlk ratio of benthic flux also exhibited sensitivity to labile material input, the bio-diffusive coefficient of O_2 , the anaerobic remineralization pathways as well as sediment porosity (Figure 8). Specifically, the DIC/TAlk ratio became much higher when aerobic processes dominated the remineralization of particulate organic matter, which was the case when the model assumed high bio-diffusive coefficients of O_2 (see benthic fluxes from BDO22 in Figures 5–7) and low labile organic material input (see benthic fluxes from Lab1 in Figures 5–7). This implies the potentially more significant role of benthic flux in acidifying bottom water over areas with high intensity of bio-diffusion. It is noteworthy that all of the calculated ratios of DIC/TAlk benthic flux exceeded 1 (Figure 8), meaning that under such bottom water condition, benthic fluxes were enhancing ocean acidification for all of the sensitivity tests.

5. Discussion

5.1. The Role of Benthic Fluxes in Bottom Water Acidification Under Fair Weather Conditions

During fair weather periods, the bottom water in the NGoM hypoxic zone has negligible bottom currents (Rabalais et al., 1994). The material exchange between the seabed and the water column plays a dominant role in controlling the biogeochemical conditions in the bottom water. In such conditions, our 1-D model results from the

YIN ET AL. 18 of 28

1942/2466, 2024, 1 (0, Downloaded from https://agupubs.onlinelibary.viley.com/doi/10.1099/2023MS040445, Wiley Online Library on [22022025]. See the Terms and Conditions (https://onlinelibrary.wiley.com/terms-and-conditions) on Wiley Online Library for rules of use; OA articles are governed by the applicable Creative Commons Licensia

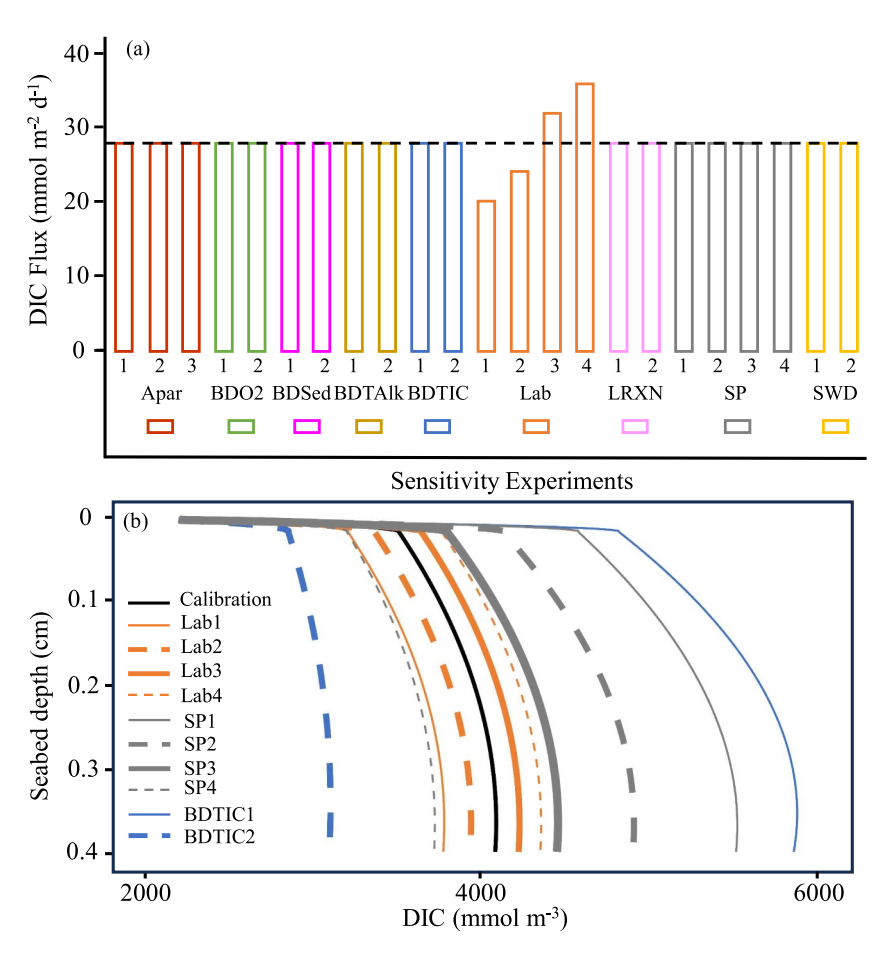


Figure 6. (a) Modeled benthic fluxes of DIC for each sensitivity experiment listed in Table 7. The black dashed line is the modeled benthic flux of DIC from the calibration run. (b) Modeled porewater concentrations of DIC. Only the results from experimental suites listed in Table 7 for which the modeled porewater concentrations were sensitive to the adjusted parameters are shown. The solid black line represents the porewater concentrations from the calibration run. In both panels (a, b) the results for the various experimental suites listed in Table 7 are in distinct colors.

calibration run and sensitivity experiments provide reasonable guidance for the role of benthic fluxes in acidifying the bottom water over the NGoM hypoxic area.

In alignment with previous observational studies (e.g., Berelson et al., 2019; Hu et al., 2017; Wang et al., 2020), our modeled DIC/TAlk ratio of benthic flux exceeded 1 (the black dashed line in Figure 8), implying that benthic fluxes play a role in acidifying the bottom water of the NGoM hypoxic zone. In addition, the sensitivity tests showed that increases in O₂ porewater concentration and penetration depth increased the proportion of particulate organic matter that was aerobically decomposed, and increased reoxidation of reduced chemical species. These would lead to an increased DIC/TAlk stoichiometry ratio compared to cases when anaerobic respiration dominates particulate organic matter decomposition and reduced products are not fully re-oxidized (e.g., Lehrter et al., 2012; Wang et al., 2020). As a result, increases in aerobic remineralization enhance the impact of seabed fluxes on bottom water acidification.

The sensitivity tests showed that the following promoted aerobic remineralization of particulate organic matter and increased the DIC/TAlk ratio of benthic flux: decreases in labile material input to the seabed, increases in the bio-diffusive coefficient of O_2 , and increases in sediment porosity (Figure 8). Normally for sediment to play an important role in bottom water acidification, both the benthic DIC flux and the DIC/TAlk ratio should be high. Therefore, we would expect the role of benthic flux in acidifying the bottom water to be significant in areas with relatively high primary production and O_2 . For the NGoM hypoxic zone, such area would be most likely found over the region where water depth ranges from \sim 20 to \sim 30 m (Figure 2b). This region represents the transition between Zone 2 and Zone 3 as defined by previous studies (e.g., Lehrter et al., 2012; Rowe & Chapman, 2002).

YIN ET AL. 19 of 28

19422466, 2024, 10, Downloaded from https://agupubs. onlinelibary.viley.com/doi/10.10.29/2023MS004045, Wiley Online Library on [22.022025]. See the Terms and Conditions (https://onlinelibrary.viley.com/terms-and-conditions) on Wiley Online Library for rules of use; OA articles are governed by the applicable Creative Com

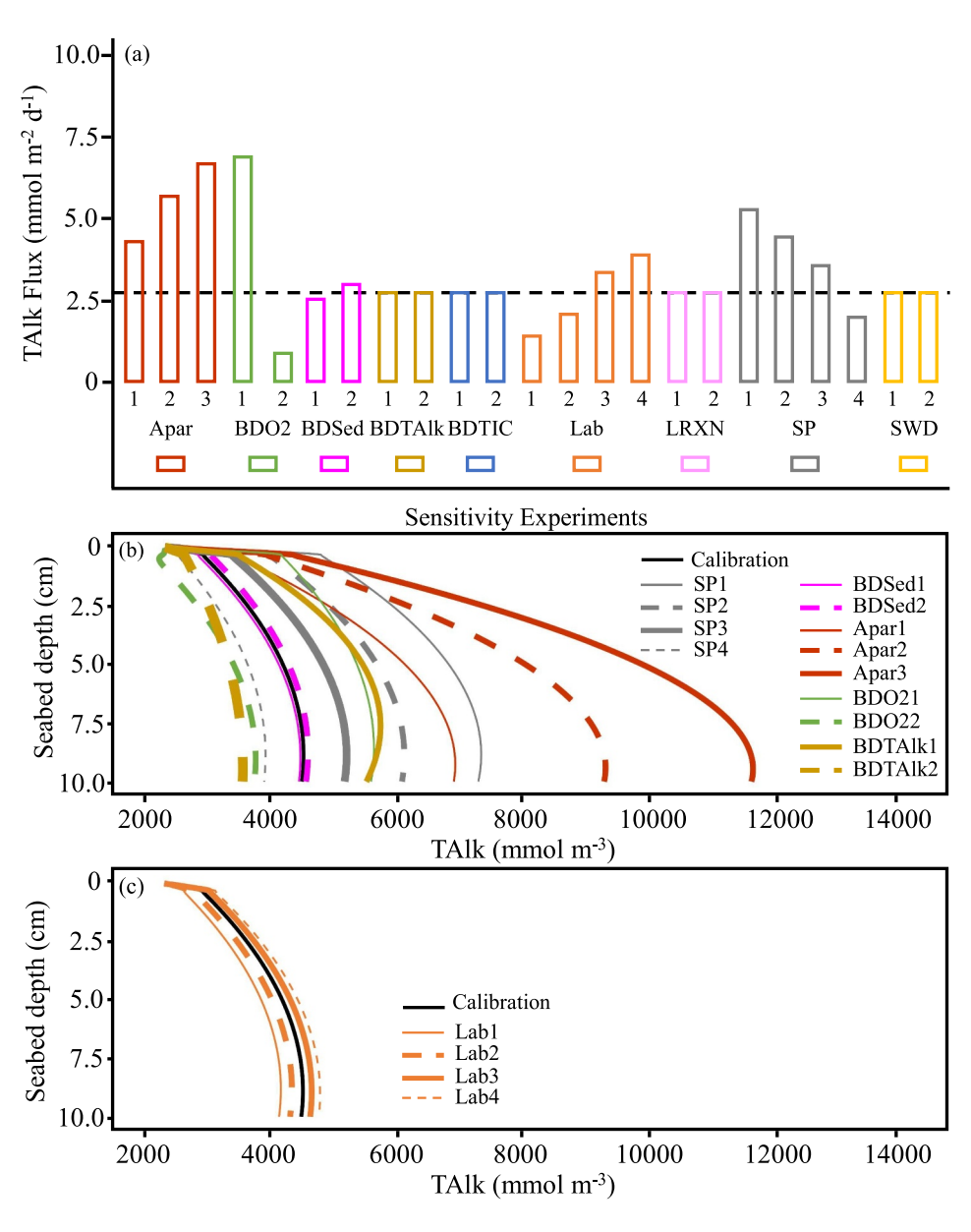


Figure 7. (a) Modeled benthic fluxes of TAlk for each sensitivity experiment listed in Table 7. The black dashed line is the modeled benthic flux of TAlk from the calibration run. (b, c) Modeled porewater concentrations of TAlk. Only the results from experimental suites listed in Table 7 for which the modeled porewater concentrations were sensitive to the adjusted parameters are shown. The solid black line represents the porewater concentrations from the calibration run. In all panels the results for the various experimental suites listed in Table 7 are in distinct colors.

The recurring acidified bottom water reported by Cai et al. (2011) and Laurent et al. (2017) was generally located in this area.

Temporally, considering the development of primary production, bottom water O_2 concentrations, and benthic faunal abundance; the role of benthic fluxes in bottom water acidification is likely to peak at the early stage of hypoxia or during the post-hypoxia period. At the early stage of hypoxia, the phytoplankton and zooplankton biomass are blooming (Fennel et al., 2011) while the oxygen level still exceeds the hypoxic threshold (Eldridge & Morse, 2008). The benthic faunal community is characterized by large number of species and high abundance before being depressed by hypoxia (Baustian et al., 2009; Gaston, 1985; Rabalais et al., 2001). For instance, Baustian (2005) reported that benthic infaunal density was 20,000 individuals/ m^2 in June prior to NGoM hypoxia and was only 1,000 individuals/ m^2 afterward. The active benthic community will favor bio-

YIN ET AL. 20 of 28

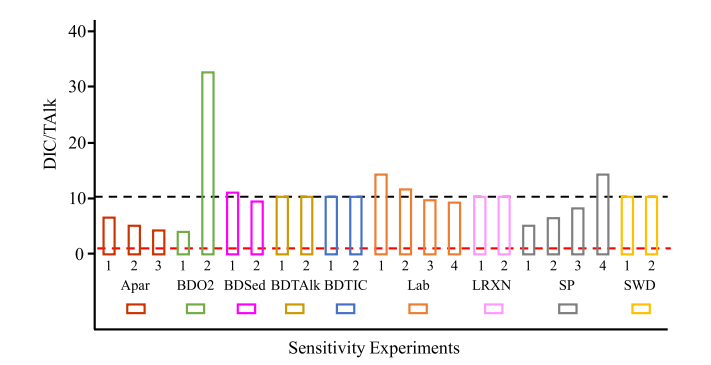


Figure 8. Modeled DIC/TAlk ratio of benthic flux for each sensitivity experiment listed in Table 7. The black dashed line is the modeled DIC/TAlk ratio of benthic flux from the calibration run. The red dashed line is the "DIC/TAlk = 1" line. Note that the results for each experimental suite listed in Table 7 are in distinct colors.

diffusion (e.g., Briggs et al., 2015; Zhang et al., 2021), and thus increase the O₂ penetration depth into the seabed. Therefore, during this period a high benthic DIC flux along with a large DIC/TAlk ratio can be expected. Similarly, as hypoxia abates, the benthic community is expected to recover (Rabalais et al., 2001), which will fuel bio-diffusion within the seabed. The increased bottom water oxygen concentrations in addition to intensified biodiffusion will contribute to the aerobic decomposition of deposited particulate matter. This will result in a high benthic DIC flux as reported by Eldridge and Morse (2008), and a large DIC/TAlk ratio, which might lead to a peak contribution of benthic flux to bottom water acidification. It should be noted that such interpretations should still hold if the model was run dynamically. This is because additional numerical experiment (not shown) in which the bottom water O₂ evolved from oxygenated (150 mmol/m³) to hypoxia (53 mmol/m³) indicate that the adjustment time of benthic fluxes to such change in bottom water O2 concentration is much shorter than the typical duration of the NGoM hypoxia.

5.2. Effect of Resuspension on Benthic DIC and TAlk Fluxes

To evaluate the role of resuspension on DIC and TAlk production, we reran our numerical model for a period that experienced strong wave- and current-induced bed shear stress (Figure 9a). Specifically, the calibrated model for Site C6 was run to represent a 50-day period that included a series of dynamic resuspension events. The wave forcing was generated from observations (significant wave height) from buoy station SPLL1 (Figure 2b) for February 19th to 9 April 2016. A periodic open momentum boundary condition was used. The current velocities vary from 1.34 m/s to 1.40 m/s. Within ROMS, the bed shear stress was calculated based on these input waves and currents following the Sherwood-Signell-Warner (SSW) bottom boundary layer closure as described in Warner et al. (2008). Using the model, we calculated the impact of resuspension on DIC and TAlk; both within the seabed and within the bottom water column (defined as the bottom 4 m).

Figure 9 shows (a) the combined wave- and current-induced bed shear stress, and fluxes of the (b) DIC, (c) TAlk and (d) O_2 for the coupled seabed-bottom water system. It should be noted that the total flux reported here was calculated as the sum of the benthic flux and that of the bottom water (i.e., the bottom 4 m).

During resuspension, previously deposited particulate organic matter was eroded from the seabed, and further deposition from the water column was inhibited. As a result, the labile material in the seabed decreased during resuspension (Figure 9e). This caused reductions in benthic fluxes of both DIC and TAlk (blue lines in Figures 9b and 9c). Meanwhile in the bottom water, resuspended particulate organic matter decomposed through the aerobic pathway, resulting in a sharp increase of DIC production and a small increase of TAlk production (brown lines in Figures 9b and 9c). When considering the coupled seabed-bottom water system, both the DIC and TAlk production were reduced during resuspension (cyan lines in Figures 9b and 9c). For instance, during resuspension Event 1 (Figure 9a), the DIC and TAlk production in the coupled seabed-bottom water were ~9% and ~28% lower than that would be released if there was no resuspension, respectively. Note that some of the particulate organic matter was resuspended above the bottom waters. A further analysis (not shown) indicates a slight increase of net DIC production during resuspension when the entire water column was considered. The reduction of the total TAlk production from the coupled seabed-bottom water system was mainly due to the transition of organic matter from being anaerobically remineralized on the seabed to being decomposed through aerobic pathway in the bottom waters after resuspension. As a result, the total O₂ consumption from the coupled seabed-bottom water system (cyan line in Figure 9d) increased during resuspension. For instance, during resuspension Event 1, mean oxygen consumption rate within the coupled seabed-bottom water system was 20% higher than that before and after resuspension.

DIC/TAlk ratio of the flux (Figure 9f) from the coupled seabed-bottom water system largely increased during the resuspension events. For instance, during the resuspension Event 1 (Figure 9a), the mean DIC/TAlk ratio was 14, which is about double its value during fair weather periods. Such an increase in DIC/TAlk ratio indicates the potential for enhanced bottom water acidification during resuspension. The reason for this increase was that resuspension entrained particulate organic matter from the seabed into the water column and hampered deposition

YIN ET AL. 21 of 28

1942/2466, 2024, 1 (0, Downloaded from https://agupubs.onlinelibary.viley.com/doi/10.1099/2023MS040445, Wiley Online Library on [22022025]. See the Terms and Conditions (https://onlinelibrary.wiley.com/terms-and-conditions) on Wiley Online Library for rules of use; OA articles are governed by the applicable Creative Commons Licensia

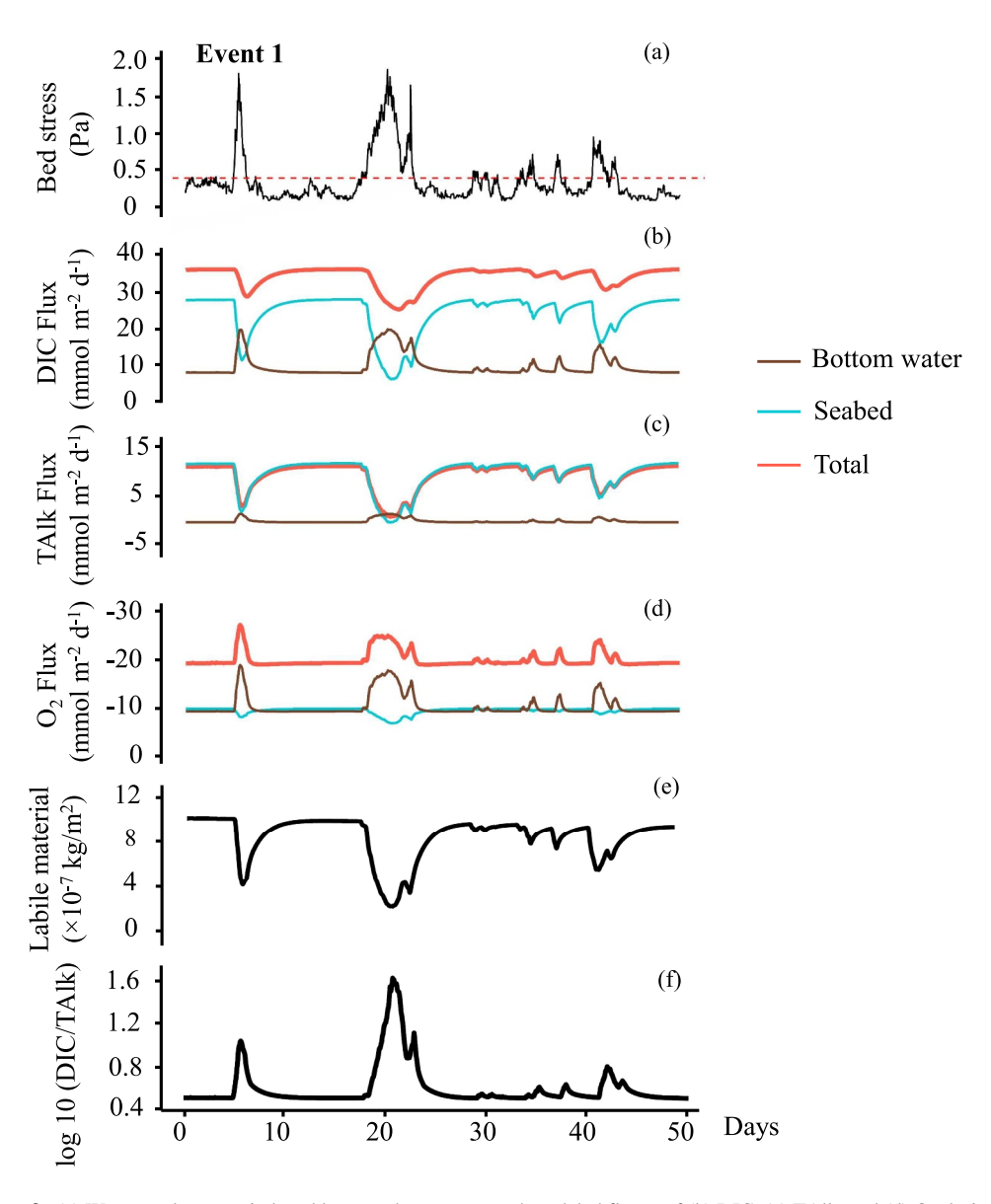


Figure 9. (a) Wave- and current-induced bottom shear stress, and modeled fluxes of (b) DIC, (c) TAlk, and (d) O₂ during a period (Feb. 19th to April 09th) that included resuspension events. (e) The mass of labile material in the top 10 cm of seabed. (f) The DIC/TAlk ratio of the newly produced DIC and TAlk in the bottom water. In panel (a), The first major resuspension event is labeled. The critical shear stress for erosion (0.4 Pa) is represented with the red dashed line. In panels (b–d) the total flux, the benthic flux and the bottom water flux are represented with solid cyan, blue and brown lines, respectively. For this analysis, "bottom water" included the bottom-most 4 m of the water column.

of organic matter. These led to longer residence times of particulate organic matter in the water column, favoring their aerobic respiration and leading to a high DIC/TAlk ratio. During the events, resuspension keeps oxygenating the water and enhances the dominance of aerobic respiration and keeping the high DIC/TAlk ratio.

Scaling up to NGoM hypoxic area, compared to the case without resuspension, we would expect resuspension would increase the dominance of the aerobic respiration in decomposing particulate organic matter, thus increasing the DIC/TAlk ratio in the coupled bottom water-seabed system and contributing to the ocean acidification. However, it should be noted that the resuspension events considered here represent medium—intensity, relatively frequent events. Thus, the results presented in this study are not representative of more intense events such as hurricanes, during which the entire water column is well mixed and seabed is largely disturbed. Understanding of benthic fluxes under resuspension conditions would benefit from extensive numerical study considering resuspension events with different intensities and durations.

YIN ET AL. 22 of 28



5.3. Model Limitations and Future Development

5.3.1. Bio-Diffusion in the Seabed

In our model, the mixing of dissolved substances in sediment is represented as a vertical diffusive process following previous studies (e.g., Sherwood et al., 2018; Soetaert et al., 1996). A limitation of this representation is that it cannot account for non-local exchange due to processes such as bio-irrigation. This may explain differences between modeled and observed porewater concentrations in the deeper sediment layers (e.g., Figure 3c). Another simplification of bio-diffusive intensity in our model is that the bio-diffusive coefficient (D_b in Equation 19) was temporally constant. Benthic infauna abundance varies largely throughout the year (Berelson et al., 2003; Brown et al., 2004; Teal et al., 2008). This variation may translate into seasonal changes to the intensity of bio-diffusion, the magnitude of which can exceed an order of magnitude (Brown et al., 2004; Teal et al., 2008). Over the NGoM hypoxic area, the intensity of the bio-diffusion is generally low year-around (Rabouille et al., 2021), and further suppressed during summer hypoxia because of largely decreased abundance, species richness and biomass of the benthic infauna (Rabalais & Baustian, 2020; Rabalais et al., 2001). As a result, the intensity of bio-diffusion, biogenic structure and microbial activity will change seasonally and during hypoxia (Briggs et al., 2015; Devereux et al., 2019), which may modify the diagenesis in the seabed and the seabed-water exchange fluxes (Devereux et al., 2019; Middelburg & Levin, 2009). In this case, use of a steady bio-diffusive coefficient may not capture seasonal variations in the intensity of bio-diffusion. However, it won't influence the validity of our conclusion on the essential role of bio-diffusion on benthic fluxes of DIC and TAlk, nor its implication to the NGoM hypoxic zone during fair-weather periods (see Section 5.1). Future model development might include a more complex representation of the benthic community to consider how the intensity of bio-diffusion changes with time and space (e.g., Zhang et al., 2021). HydroBioSed is well-equipped for use in these studies because it could be modified to account for the spatial and temporal variations in the bio-diffusive coefficient.

5.3.2. Calcium Carbonate Cycling

In the NGOM hypoxic zone, the content of calcium carbonate in the NGOM hypoxic zone seabed sediment is low, with an averaged mass content of inorganic carbon 0.5% (Gordon & Goni, 2004). In addition, the porewaters were reported to be saturated with calcite in surface sediments (Berelson et al., 2019; Rabouille et al., 2021) and the porewater profile of calcite showed minimal change with depth (Berelson et al., 2019), which does not support the occurrence of calcium carbonate dissolution and precipitation. Thus, the contributions of calcium carbonate dissolution and precipitation to benthic DIC and TAlk fluxes should be limited and therefore not represented in our model.

However, calcium carbonate cycling can be an important process affecting benthic DIC and TAlk fluxes, as well as the associated DIC/TAlk ratio. Dissolution of 1 mol calcium carbonate generates 1 mol DIC and leads to 2 mol equivalents increase of TAlk. The carbonate precipitation on the other hand can act as a sink for TAlk. Globally, particulate organic matter decomposition in shallow marine sediments can cause a 7 Tmol carbonate dissolution per year, resulting in a 13.14 Teq TAlk release to the water column (Krumins et al., 2013). In the North Sea, carbonate dissolution in sediments can release up to 5.4 mmol m^{-2} d⁻¹ of TAlk (Brenner et al., 2016). Future effort to include the calcium carbonate cycling in the model would be useful for applying the model over systems where it is important for benthic DIC and TAlk fluxes.

5.3.3. Effects of Coupled Sulfate Reduction and Iron Sulfide Burial

The reduction of 1 mol SO_4^{2-} and Fe oxides can produce 2 mol TAlk. The reoxidation of 1 mol Fe^{2+} and S^{2+} can remove 2 mol TAlk. Thus, there is no net TAlk generation when the reductions of SO_4^{2-} and Fe oxides are coupled with the reoxidation of the reduced species. However, the SO_4^{2-} reduction can lead to a net TAlk production when the produced sulfide reacts with Fe^{2+} to form FeS and get buried as Fe sulfide minerals (Hu & Cai, 2011). The coupling between SO_4^{2-} reduction and Fe sulfide burial is reported to generate a TAlk flux of 44 Gmol/yr in the Baltic Proper, which accounts for up to 26% of the missing TAlk source in this basin (Gustafsson et al., 2019).

Fe and S are not explicitly represented in the current model presented. Part of the reason is that the measurements of S, Fe and SO_4^{2-} for model calibration are not available. Thus, we didn't explore the possible impact of Fe sulfide deposition on TAlk generation in this study. However, the formation of the solid-phase species from

YIN ET AL. 23 of 28

oxygen demand units (ODU: Mn²⁺, Fe²⁺ and S²⁺) are considered using the parameter PB following Soetaert et al. (1996). PB represents the proportion of ODU that forms as solids (Table 3). This process affects the calculations of ODU concentration (Equation 16), and TAlk production (Equation 18) due to ODU reoxidation (Figure 1) in the model.

5.3.4. Site-Specific to Regional Scale

Upscaling the site-specific simulation to regional scale is important for quantifying the benthic fluxes at system scales. Previous studies have documented the coupling between site specific sediment models with regional models. In Gustafsson et al. (2019), the benthic TAlk flux due to S burial at a specific site that is computed by a 1-D sediment reactive-transport model RTM (Reed et al., 2016) was upscaled to the whole basin by multiplying simulated TAlk flux by the total muddy sediment area of the basin. The assumption is that the RTM calculated benthic TAlk flux is representative for the muddy sediment area. In Archer et al. (2002), the Muds model was used to simulate the global sedimentary carbon cycle. In the application, the overlying water chemistry and organic carbon flux into the sediment were extracted from global gridded water column data sets and imposed as boundary conditions for the seabed diagenetic model. Remineralization rates were parameterized as functions of organic carbon flux. An oxygen-differentiated hypsometry of the seabed was used to consider the contributions of seabed with different overlying water oxygen concentrations and depth to global carbon burial. These approaches do not simulate the three-dimensional hydrodynamics and do not account for its effect on the benthic fluxes.

Other approaches have used sediment diagenetic models within the framework of a three-dimensional hydrodynamic ocean model (e.g., Testa et al., 2014). In fact, HydroBioSed has been used this way within both Chesapeake Bay and the NGoM (Moriarty et al., 2018, 2021). HydroBioSed can be applied in 3-D to realistically represent the spatial-temporally varying hydrodynamics, water column biogeochemistry, seabed diagenesis and the benthic-pelagic interactions. While these previous implementations of HydroBioSed did not account for TAlk or DIC, they did account for the diagenetic processes in addition to particulate matter resuspension, transport, and deposition. In the present study, HydroBioSed was applied in 1-D (vertical) at two sites in NGoM hypoxic zone. Results from the 1-D model quantified the contribution of benthic fluxes in acidifying the bottom water at these two sites with reasonable accuracy and provided guidance for the role of benthic fluxes in ocean acidification over the NGoM hypoxic zone. However, to realistically simulate the benthic-pelagic interaction over the NGoM hypoxic zone and quantify the role of benthic flux in ocean acidification at regional scales would require a 3-D application of HydroBioSed. This motivates future work to run the 3-D implementation of HydroBioSed at regional scale now that it accounts for changes in TAlk and DIC. Finally, HydroBioSed has been developed within widely used community ocean models, COAWST and ROMS. This facilitates scaling from the onedimensional (vertical) site-specific implementations shown in this paper to the regional scales within threedimensional implementations that account for hydrodynamics, sediment transport and resuspension, and biogeochemical processes (e.g., Moriarty et al., 2018, 2021).

6. Summary and Conclusions

This paper describes a coupled benthic-pelagic model for estimating the exchanges of particulates and solutes between the seabed and the water column. This model, HydroBioSed, was initially developed by Moriarty et al. (2017, 2018, 2021). As described in this paper, we subsequently expanded the model functionality by adding algorithms to represent benthic DIC and TAlk. In addition, the representation of the anaerobic remineralization in the seabed was improved by including manganese- and iron-oxides reduction, and sulfate reduction. Thus, the model presented in this paper can simulate the exchange of particulate organic matter, O₂, NO₃, NH₄, DIC, TAlk between the seabed and the water column. Test cases for two locations in the NGoM hypoxic zone demonstrated the capability of the model to reproduce both the porewater concentrations and benthic fluxes of the solutes mentioned above.

With the newly added formulae for DIC and TAlk dynamics in the coupled benthic-pelagic model, this paper explored the potential role of benthic fluxes in acidifying the bottom water during both quiescent and episodic resuspension periods over the NGoM hypoxic zone. During fair weather periods, factors affecting the relative availability of oxygen in the seabed had a large control on the modeled DIC/TAlk ratio of benthic fluxes; these factors included bio-diffusion, labile material input and sediment porosity. Scaling up to the NGoM hypoxic zone,

YIN ET AL. 24 of 28

19422466, 2024, 10, Downloaded from https://agupubs.onlinelibrary.wiley.com/doi/10.1029/2023MS004045, Wiley Online Library on [22/02/2025]. See the Terms and Conditions

we believe benthic fluxes to play an important role in acidifying bottom water over the transition area of the previously classified Zone 2 and Zone 3 of the NGoM hypoxic zone, where water depth ranges from \sim 20 to \sim 30 m (Lehrter et al., 2012 or Rowe & Chapman, 2002). Temporally, considering the development of primary production, bottom water concentration as well as benthic fauna abundance, the role of benthic fluxes in acidifying the bottom water likely peak at the early stages of hypoxia or during post-hypoxia periods. When the model was run to represent periods of resuspension, we calculated a small decrease in DIC production, but a large increase in the DIC/TAlk ratio. This confirmed the role of resuspension in enhancing bottom water acidification.

Data Availability Statement

The observation data used in this study is shared with the supplementary material (Tables S1–S3 in Supporting Information S1). Model data sets are publicly available through the William & Mary Scholar Works (https://www.doi.org/10.25773/ajk6-4b53, Yin et al., 2024).

Acknowledgments References

The authors thank Dr. Wei-Jun Cai (University of Delaware) for important advice on the model application. Funding for this research was provided by National Science Foundation Chemical Oceanography Program (OCE–1756576 and OCE-1756788). The authors acknowledge William & Mary Research Computing for providing computational resources and technical support that have contributed to the results reported within this paper. Input from three anonymous reviewers is appreciated and we believe

helped to strengthen the paper.

- Aller, R. C. (1998). Mobile deltaic and continental shelf muds as suboxic, fluidized bed reactors. *Marine Chemistry*, 61(3–4), 143–155. https://doi.org/10.1016/S0304-4203(98)00024-3
- Allison, M. A., Kineke, G. C., Gordon, E. S., & Goni, M. A. (2000). Development and reworking of a seasonal flood deposit on the inner continental shelf off the Atchafalaya River. *Continental Shelf Research*, 20(16), 2267–2294. https://doi.org/10.1016/S0278-4343(00)00070-4 Anthony, K. R. N., Diaz-Pulido, G., Verlinden, N., Tilbrook, B., & Andersson, A. J. (2013). Benthic buffers and boosters of ocean acidification on
- coral reefs. *Biogeosciences*, 10(7), 4897–4909. https://doi.org/10.5194/bg-10-4897-2013

 Archer, D. E., Morford, J. L., & Emerson, S. R. (2002). A model of suboxic sedimentary diagenesis suitable for automatic tuning and gridded global domains. *Global Biogeochemical Cycles*, 16(1), 17–21. https://doi.org/10.1029/2000gb001288
- Arzayus, K. M., & Canuel, E. A. (2005). Organic matter degradation in sediments of the York River estuary: Effects of biological vs. physical mixing. *Geochimica et Cosmochimica Acta*, 69(2), 455–464. https://doi.org/10.1016/j.gca.2004.06.029
- Baustian, M. M. (2005). Benthic communities in the Northern Gulf of Mexico hypoxic area: Potential prey for demersal fish, (master's thesis).

 Retrieved from LSU digital commons LSU digital commons. Louisiana State University and Agricultural & Mechanical College. Retrieved from https://digitalcommons.lsu.edu/gradschool_theses/2766/
- Baustian, M. M., Craig, J. K., & Rabalais, N. N. (2009). Effects of summer 2003 hypoxia on macrobenthos and Atlantic croaker foraging selectivity in the Northern Gulf of Mexico. *Journal of Experimental Marine Biology and Ecology*, 381, S31–S37. https://doi.org/10.1016/j.jembe.2009.07.007
- Berelson, W., McManus, J., Coale, K., Johnson, K., Burdige, D., Kilgore, T., et al. (2003). A time series of benthic flux measurements from Monterey Bay, CA. Continental Shelf Research, 23(5), 457–481. https://doi.org/10.1016/s0278-4343(03)00009-8
- Berelson, W. M., McManus, J., Coale, K. H., Johnson, K. S., Kilgore, T., Burdige, D., & Pilskaln, C. (1996). Biogenic matter diagenesis on the sea floor: A comparison between two continental margin transects. *Journal of Marine Research*, 54(4), 731–762. https://doi.org/10.1357/0022240963213673
- Berelson, W. M., McManus, J., Severmann, S., & Rollins, N. (2019). Benthic fluxes from hypoxia-influenced Gulf of Mexico sediments: Impact on bottom water acidification. *Marine Chemistry*, 209, 94–106. https://doi.org/10.1016/j.marchem.2019.01.004
- Boynton, W. R., Ceballos, M. A. C., Bailey, E. M., Hodgkins, C. L. S., Humphrey, J. L., & Testa, J. M. (2018). Oxygen and nutrient exchanges at the sediment-water interface: A global synthesis and critique of estuarine and coastal data. *Estuaries and Coasts*, 41(2), 301–333. https://doi.org/10.1007/s12237-017-0275-5
- Brenner, H., Braeckman, U., Le Guitton, M., & Meysman, F. J. (2016). The impact of sedimentary alkalinity release on the water column CO₂ system in the North Sea. *Biogeosciences*, 13(3), 841–863. https://doi.org/10.5194/bg-13-841-2016
- Briggs, K. B., Hartmann, V. A., Yeager, K. M., Shivarudrappa, S., Díaz, R. J., Osterman, L. E., & Reed, A. H. (2015). Influence of hypoxia on biogenic structure in sediments on the Louisiana continental shelf. *Estuarine, Coastal and Shelf Science*, 164, 147–160. https://doi.org/10.1016/j.ecss.2015.07.019
- Brown, J. H., Gillooly, J. F., Allen, A. P., Savage, V. M., & West, G. B. (2004). Toward a metabolic theory of ecology. *Ecology*, 85(7), 1771–1789. https://doi.org/10.1890/03-9000
- Cai, W. J., Hu, X., Huang, W. J., Murrell, M. C., Lehrter, J. C., Lohrenz, S. E., et al. (2011). Acidification of subsurface coastal waters enhanced by eutrophication. *Nature Geoscience*, 4(11), 766–770. https://doi.org/10.1038/ngeo1297
- Cai, W. J., & Sayles, F. L. (1996). Oxygen penetration depths and fluxes in marine sediments. Marine Chemistry, 52(2), 123–131. https://doi.org/10.1016/0304-4203(95)00081-X
- Canfield, D. E., Jørgensen, B. B., Fossing, H., Glud, R., Gundersen, J., Ramsing, N. B., et al. (1993). Pathways of organic carbon oxidation in three continental margin sediments. *Marine Geology*, 113(1–2), 27–40. https://doi.org/10.1016/0025-3227(93)90147-N
- Corbett, D. R., McKee, B., & Duncan, D. (2004). An evaluation of mobile mud dynamics in the Mississippi River deltaic region. *Marine Geology*, 209(1–4), 91–112. https://doi.org/10.1016/j.margeo.2004.05.028
- Cowie, G., & Woulds, C. (2011). Tracer studies of benthic communities and biogeochemical processes in coastal and estuarine marine environments. In E. Wolanski & D. McLusky (Eds.), *Treatise on estuarine and coastal science. Vol 4: Geochemistry of estuaries and coasts* (pp. 39–70). Elsevier Academic Press Inc.
- Devereux, R., Lehrter, J. C., Beddick Jr, D. L., Yates, D. F., & Jarvis, B. M. (2015). Manganese, iron, and sulfur cycling in Louisiana continental shelf sediments. *Continental Shelf Research*, 99, 46–56. https://doi.org/10.1016/j.csr.2015.03.008
- Devereux, R., Lehrter, J. C., Cicchetti, G., Beddick, D. L., Yates, D. F., Jarvis, B. M., et al. (2019). Spatially variable bioturbation and physical mixing drive the sedimentary biogeochemical seascape in the Louisiana continental shelf hypoxic zone. *Biogeochemistry*, 143(2), 151–169. https://doi.org/10.1007/s10533-019-00539-8
- Dunne, J. P., Sarmiento, J. L., & Gnanadesikan, A. (2007). A synthesis of global particle export from the surface ocean and cycling through the ocean interior and on the seafloor. *Global Biogeochemical Cycles*, 21(4). https://doi.org/10.1029/2006GB002907

YIN ET AL. 25 of 28



Journal of Advances in Modeling Earth Systems

- 10.1029/2023MS004045
- Egleston, E. S., Sabine, C. L., & Morel, F. M. (2010). Revelle revisited: Buffer factors that quantify the response of ocean chemistry to changes in DIC and alkalinity. *Global Biogeochemical Cycles*, 24(1). https://doi.org/10.1029/2008GB003407
- Eldridge, P. M., & Morse, J. W. (2008). Origins and temporal scales of hypoxia on the Louisiana shelf: Importance of benthic and sub-pycnocline water metabolism. *Marine Chemistry*, 108(3–4), 159–171. https://doi.org/10.1016/j.marchem.2007.11.009
- Evans, G. T., & Parslow, J. S. (1985). A model of annual plankton cycles. *Biological Oceanography*, 3(3), 327–347. https://doi.org/10.1080/01965581.1985.10749478
- Fennel, K., Hetland, R., Feng, Y., & DiMarco, S. (2011). A coupled physical-biological model of the Northern Gulf of Mexico shelf: Model description, validation and analysis of phytoplankton variability. *Biogeosciences*, 8(7), 1881–1899. https://doi.org/10.5194/bg-8-1881-2011
- Fennel, K., Hu, J., Laurent, A., Marta-Almeida, M., & Hetland, R. (2013). Sensitivity of hypoxia predictions for the Northern Gulf of Mexico to sediment oxygen consumption and model nesting. *Journal of Geophysical Research: Oceans*, 118(2), 990–1002. https://doi.org/10.1002/jgrc. 20077
- Fennel, K., & Testa, J. M. (2019). Biogeochemical controls on coastal hypoxia. Annual Review of Marine Science, 11(1), 105–130. https://doi.org/10.1146/annurev-marine-010318-095138
- Fennel, K., Wilkin, J., Levin, J., Moisan, J., O'Reilly, J., & Haidvogel, D. (2006). Nitrogen cycling in the Middle Atlantic Bight: Results from a three-dimensional model and implications for the North Atlantic nitrogen budget. *Global Biogeochemical Cycles*, 20(3). https://doi.org/10.1029/2005GB002456
- Fennel, K., Wilkin, J., Previdi, M., & Najjar, R. (2008). Denitrification effects on air-sea CO₂ flux in the coastal ocean: Simulations for the northwest North Atlantic. *Geophysical Research Letters*, 35(24). https://doi.org/10.1029/2008GL036147
- Garcia, H. E., & Gordon, L. I. (1992). Oxygen solubility in seawater: Better fitting equations. Limnology & Oceanography, 37(6), 1307–1312. https://doi.org/10.4319/lo.1992.37.6.1307
- Gaston, G. R. (1985). Effects of hypoxia on macrobenthos of the inner shelf off Cameron, Louisiana. Estuarine, Coastal and Shelf Science, 20(5), 603–613. https://doi.org/10.1016/0272-7714(85)90110-6
- Gomez, F. A., Lee, S. K., Liu, Y., Hernandez Jr, F. J., Muller-Karger, F. E., & Lamkin, J. T. (2018). Seasonal patterns in phytoplankton biomass across the northern and deep Gulf of Mexico: A numerical model study. *Biogeosciences*, 15(11), 3561–3576. https://doi.org/10.5194/bg-15-3561-2018
- Gordon, E. S., & Goni, M. A. (2004). Controls on the distribution and accumulation of terrigenous organic matter in sediments from the Mississippi and Atchafalaya river margin. *Marine Chemistry*, 92(1–4), 331–352. https://doi.org/10.1016/j.marchem.2004.06.035
- Gustafsson, E., Hagens, M., Sun, X., Reed, D. C., Humborg, C., Slomp, C. P., & Gustafsson, B. G. (2019). Sedimentary alkalinity generation and long-term alkalinity development in the Baltic Sea. *Biogeosciences*, 16(2), 437–456. https://doi.org/10.5194/bg-16-437-2019
- Haidvogel, D. B., Arango, H., Budgell, W. P., Cornuelle, B. D., Curchitser, E., Di Lorenzo, E., et al. (2008). Ocean forecasting in Terrain-following coordinates: Formulation and skill assessment of the regional Ocean modeling system. *Journal of Computational Physics*, 227(7), 3595–3624. https://doi.org/10.1016/j.jcp.2007.06.016
- Haidvogel, D. B., Arango, H. G., Hedstrom, K., Beckmann, A., Malanotte-Rizzoli, P., & Shchepetkin, A. F. (2000). Model evaluation experiments in the North Atlantic basin: Simulations in nonlinear Terrain-following coordinates. *Dynamics of Atmospheres and Oceans*, 32(3–4), 239–281. https://doi.org/10.1016/S0377-0265(00)00049-X
- Hartnett, H. E., Keil, R. G., Hedges, J. I., & Devol, A. H. (1998). Influence of oxygen exposure time on organic carbon preservation in continental margin sediments. *Nature*, 391(6667), 572–575. https://doi.org/10.1038/35351
- Heip, C. H. R., Goosen, N. K., Herman, P. M. J., Kromkamp, J., Middelburg, J. J., & Soetaert, K. (1995). Production and consumption of biological particles in temperate tidal estuaries. Oceanography and Marine Biology an Annual Review, 33, 1–149.
- Hopkinson, C. S., Jr. (1985). Shallow-water benthic and pelagic metabolism: Evidence of heterotrophy in the nearshore Georgia Bight. *Marine Biology*, 87(1), 19–32. https://doi.org/10.1007/BF00397002
- Hu, X., & Cai, W. J. (2011). The impact of denitrification on the atmospheric CO₂ uptake potential of seawater. *Marine Chemistry*, 127(1–4), 192–198. https://doi.org/10.1016/j.marchem.2011.09.008
- Hu, X., Li, Q., Huang, W. J., Chen, B., Cai, W. J., Rabalais, N. N., & Turner, R. E. (2017). Effects of eutrophication and benthic respiration on water column carbonate chemistry in a traditional hypoxic zone in the Northern Gulf of Mexico. *Marine Chemistry*, 194, 33–42. https://doi.org/10.1016/j.marchem.2017.04.004
- Hülse, D., Arndt, S., Daines, S., Regnier, P., & Ridgwell, A. (2018). OMEN-SED 1.0: A novel, numerically efficient organic matter sediment diagenesis module for coupling to Earth system models. Geoscientific Model Development, 11(7), 2649–2689. https://doi.org/10.5194/gmd-11-2649-2018
- Jorgensen, B. B., Bang, M., & Blackburn, T. H. (1990). Anaerobic mineralization in marine sediments from the Baltic Sea-North Sea transition. Marine Ecology Progress Series, 59, 39–54. https://doi.org/10.3354/MEPS059039
- Justić, D., Rabalais, N. N., & Turner, R. E. (2002). Modeling the impacts of decadal changes in riverine nutrient fluxes on coastal eutrophication near the Mississippi River Delta. Ecological Modelling, 152(1), 33–46. https://doi.org/10.1016/S0304-3800(01)00472-0
- Kemp, W. M., Sampou, P. A., Garber, J., Tuttle, J., & Boynton, W. R. (1992). Seasonal depletion of oxygen from bottom waters of Chesapeake Bay: Roles of benthic and planktonic respiration and physical exchange processes. *Marine Ecology Progress Series*, 85, 137–152. https://doi. org/10.3354/MEPS085137
- Krumins, V., Gehlen, M., Arndt, S., Van Cappellen, P., & Regnier, P. (2013). Dissolved inorganic carbon and alkalinity fluxes from coastal marine sediments: Model estimates for different shelf environments and sensitivity to global change. *Biogeosciences*, 10(1), 371–398. https://doi.org/10.5194/bg-10-371-2013
- Laurent, A., Fennel, K., Cai, W. J., Huang, W. J., Barbero, L., & Wanninkhof, R. (2017). Eutrophication-induced acidification of coastal waters in the Northern Gulf of Mexico: Insights into origin and processes from a coupled physical-biogeochemical model. *Geophysical Research Letters*, 44(2), 946–956. https://doi.org/10.1002/2016GL071881
- Lehrter, J. C., Beddick, D. L., Devereux, R., Yates, D. F., & Murrell, M. C. (2012). Sediment-water fluxes of dissolved inorganic carbon, O₂, nutrients, and N₂ from the hypoxic region of the Louisiana continental shelf. *Biogeochemistry*, 109(1–3), 233–252. https://doi.org/10.1007/s10533-011-9623-x
- Middelburg, J. J., & Levin, L. A. (2009). Coastal hypoxia and sediment biogeochemistry. *Biogeosciences*, 6(7), 1273–1293. https://doi.org/10.5194/bg-6-1273-2009
- Middelburg, J. J., & Soetaert, K. (2004). The role of sediments in shelf ecosystem dynamics. In A. R. Robinson & K. Brink (Eds.), The global coastal ocean: Multiscale interdisciplinary processes (pp. 353–374). Harvard University Press.
- Moriarty, J. M., Friedrichs, M. A., & Harris, C. K. (2021). Seabed resuspension in the Chesapeake Bay: Implications for biogeochemical cycling and hypoxia. *Estuaries and Coasts*, 44(1), 103–122. https://doi.org/10.1007/s12237-020-00763-8

YIN ET AL. 26 of 28

- Moriarty, J. M., Harris, C. K., Fennel, K., Friedrichs, M. A., Xu, K., & Rabouille, C. (2017). The roles of resuspension, diffusion and biogeochemical processes on oxygen dynamics offshore of the Rhône river, France: A numerical modeling study. *Biogeosciences*, 14(7), 1919–1946. https://doi.org/10.5194/bg-14-1919-2017
- Moriarty, J. M., Harris, C. K., Friedrichs, M. A., Fennel, K., & Xu, K. (2018). Impact of seabed resuspension on oxygen and nitrogen dynamics in the Northern Gulf of Mexico: A numerical modeling study. *Journal of Geophysical Research: Oceans*, 123(10), 7237–7263. https://doi.org/10.1029/20181C013950
- Morse, J. W., & Eldridge, P. M. (2007). A non-steady state diagenetic model for changes in sediment biogeochemistry in response to seasonally hypoxic/anoxic conditions in the "dead zone" of the Louisiana shelf. *Marine Chemistry*, 106(1–2), 239–255. https://doi.org/10.1016/j.marchem.2006.02.003
- Murrell, M. C., & Lehrter, J. C. (2011). Sediment and lower water column oxygen consumption in the seasonally hypoxic region of the Louisiana continental shelf. *Estuaries and Coasts*, 34(5), 912–924. https://doi.org/10.1007/s12237-010-9351-9
- Nunnally, C. C., Quigg, A., DiMarco, S., Chapman, P., & Rowe, G. T. (2014). Benthic–pelagic coupling in the Gulf of Mexico hypoxic area: Sedimentary enhancement of hypoxic conditions and near bottom primary production. *Continental Shelf Research*, 85, 143–152. https://doi.org/10.1016/j.csr.2014.06.006
- Rabalais, N. N., & Baustian, M. M. (2020). Historical shifts in benthic infaunal diversity in the Northern Gulf of Mexico since the appearance of seasonally severe hypoxia. *Diversity*, 12(2), 49. https://doi.org/10.3390/d12020049
- Rabalais, N. N., Smith, L. E., Harper Jr, D. E., & Justic, D. (2001). Effects of seasonal hypoxia on continental shelf benthos. In N. N. Rabalais & R. E. Turner (Eds.), Coastal and estuarine studies: Coastal hypoxia: Consequences for living resources and ecosystems (pp. 211–240). American Geophysical Union.
- Rabalais, N. N., Wiseman, W. J., & Turner, R. E. (1994). Comparison of continuous records of near-bottom dissolved oxygen from the hypoxia zone along the Louisiana coast. *Estuaries*, 17(4), 850–861. https://doi.org/10.2307/1352753
- Rabouille, C., Lansard, B., Owings, S. M., Rabalais, N. N., Bombled, B., Metzger, E., et al. (2021). Early diagenesis in the hypoxic and acidified zone of the Northern Gulf of Mexico: Is organic matter recycling in sediments disconnected from the water column? Frontiers in Marine Science, 8, 604330, https://doi.org/10.3389/fmars.2021.604330
- Rasmussen, H., & Jørgensen, B. B. (1992). Microelectrode studies of seasonal oxygen uptake in a coastal sediment: Role of molecular diffusion. Marine Ecology Progress Series, 81(3), 289–303. https://doi.org/10.3354/meps081289
- Reed, D. C., Gustafsson, B. G., & Slomp, C. P. (2016). Shelf-to-basin iron shuttling enhances vivianite formation in deep Baltic Sea sediments. Earth and Planetary Science Letters, 434, 241–251. https://doi.org/10.1016/j.epsl.2015.11.033
- Roden, E. E., & Tuttle, J. H. (1992). Sulfide release from estuarine sediments underlying anoxic bottom water. Limnology & Oceanography, 37(4), 725–738. https://doi.org/10.4319/lo.1992.37.4.0725
- Rowe, G. T., & Chapman, P. (2002). Continental shelf hypoxia: Some nagging questions. Gulf of Mexico Science, 20(2), 8. https://doi.org/10.
- Shchepetkin, A. F., & McWilliams, J. C. (2003). A method for computing horizontal pressure-gradient force in an oceanic model with a nonaligned vertical coordinate. *Journal of Geophysical Research*, 108(C3). https://doi.org/10.1029/2001JC001047
- Shchepetkin, A. F., & McWilliams, J. C. (2009). Correction and commentary for "Ocean forecasting in terrain-following coordinates: Formulation and skill assessment of the regional ocean modeling system" by Haidvogel et al., J. Comp. Phys. 227, pp. 3595–3624. *Journal of Computational Physics*, 228(24), 8985–9000. https://doi.org/10.1016/j.jcp.2009.09.002
- Sherwood, C. R., Aretxabaleta, A. L., Harris, C. K., Rinehimer, J. P., Verney, R., & Ferré, B. (2018). Cohesive and mixed sediment in the regional ocean modeling system (ROMS v3. 6) implemented in the Coupled Ocean–Atmosphere–Wave–Sediment Transport Modeling System (COAWST r1234). Geoscientific Model Development, 11(5), 1849–1871. https://doi.org/10.5194/gmd-11-1849-2018
- Soetaert, K., Herman, P. M., & Middelburg, J. J. (1996). A model of early diagenetic processes from the shelf to abyssal depths. *Geochimica et Cosmochimica Acta*, 60(6), 1019–1040. https://doi.org/10.1016/0016-7037(96)00013-0
- Ståhlberg, C., Bastviken, D., Svensson, B. H., & Rahm, L. (2006). Mineralisation of organic matter in coastal sediments at different frequency and duration of resuspension. *Estuarine, Coastal and Shelf Science*, 70(1–2), 317–325. https://doi.org/10.1016/j.ecss.2006.06.022
- Suess, E. (1980). Particulate organic carbon flux in the oceans-surface productivity and oxygen utilization. *Nature*, 288(5788), 260–263. https://doi.org/10.1038/288260a0
- Teal, L. R., Bulling, M. T., Parker, E. R., & Solan, M. (2008). Global patterns of bioturbation intensity and mixed depth of marine soft sediments. Aquatic Biology, 2(3), 207–218. https://doi.org/10.3354/ab00052
- Tengberg, A., Almroth, E., & Hall, P. (2003). Resuspension and its effects on organic carbon recycling and nutrient exchange in coastal sediments: In situ measurements using new experimental technology. *Journal of Experimental Marine Biology and Ecology*, 285, 119–142. https://doi.org/10.1016/S0022-0981(02)00523-3
- Testa, J. M., Li, Y., Lee, Y. J., Li, M., Brady, D. C., Di Toro, D. M., et al. (2014). Quantifying the effects of nutrient loading on dissolved O₂ cycling and hypoxia in Chesapeake Bay using a coupled hydrodynamic–biogeochemical model. *Journal of Marine Systems*, 139, 139–158. https://doi.org/10.1016/j.jmarsys.2014.05.018
- Turner, R. E., Rabalais, N. N., & Justic, D. (2008). Gulf of Mexico hypoxia: Alternate states and a legacy. *Environmental Science & Technology*, 42(7), 2323–2327. https://doi.org/10.1021/es071617k
- Van Cappellen, P., & Wang, Y. (1996). Cycling of iron and manganese in surface sediments; a general theory for the coupled transport and reaction of carbon, oxygen, nitrogen, sulfur, iron, and manganese. American Journal of Science, 296(3), 197–243. https://doi.org/10.2475/ajs. 296.3.197
- Wainright, S. C., & Hopkinson, C. S., Jr. (1997). Effects of sediment resuspension on organic matter processing in coastal environments: A simulation model. *Journal of Marine Systems*, 11(3–4), 353–368. https://doi.org/10.1016/S0924-7963(96)00130-3
- Wang, H., Lehrter, J., Maiti, K., Fennel, K., Laurent, A., Rabalais, N., et al. (2020). Benthic respiration in hypoxic waters enhances bottom water acidification in the Northern Gulf of Mexico. *Journal of Geophysical Research: Oceans*, 125(10), e2020JC016152. https://doi.org/10.1029/ 2020JC016152
- Wanninkhof, R. (1992). Relationship between wind speed and gas exchange over the ocean. *Journal of Geophysical Research*, 97(C5), 7373–7382. https://doi.org/10.1029/92JC00188
- Warner, J. C., Armstrong, B., He, R., & Zambon, J. B. (2010). Development of a coupled ocean-atmosphere-wave-sediment transport (COAWST) modeling system. *Ocean Modelling*, 35(3), 230–244. https://doi.org/10.1016/j.ocemod.2010.07.010
- Warner, J. C., Sherwood, C. R., Signell, R. P., Harris, C. K., & Arango, H. G. (2008). Development of a three-dimensional, regional, coupled wave, current, and sediment-transport model. *Computers & Geosciences*, 34(10), 1284–1306. https://doi.org/10.1016/j.cageo.2008.02.012
- Xu, K., Harris, C. K., Hetland, R. D., & Kaihatu, J. M. (2011). Dispersal of Mississippi and Atchafalaya sediment on the Texas–Louisiana shelf: Model estimates for the year 1993. Continental Shelf Research, 31(15), 1558–1575. https://doi.org/10.1016/j.csr.2011.05.008

YIN ET AL. 27 of 28

- Yin, D., Cui, L., Harris, C. K., Moriarty, J. M., Beck, H., & Maiti, K. (2024). A model archive for an updated water column biogeochemical-seabed diagenetic and sediment transport model for the Northern Gulf of Mexico hypoxic zone [Dataset]. William & Mary Scholar Works. https://doi.org/10.25773/ajk6-4b53
- Yu, L., Fennel, K., Laurent, A., Murrell, M. C., & Lehrter, J. C. (2015). Numerical analysis of the primary processes controlling oxygen dynamics on the Louisiana shelf. *Biogeosciences*, 12(7), 2063–2076. https://doi.org/10.5194/bg-12-2063-2015
- Zhang, W., Neumann, A., Daewel, U., Wirtz, K., van Beusekom, J. E., Eisele, A., et al. (2021). Quantifying importance of macrobenthos for benthic-pelagic coupling in a temperate coastal shelf sea. *Journal of Geophysical Research: Oceans*, 126(10), e2020JC016995. https://doi.org/10.1029/2020JC016995

YIN ET AL. 28 of 28